

Dimers for Type D Relativistic Toda Model

Kimyeong Lee^a and Norton Lee^b

^a*School of Physics, Korea Institute for Advanced Study,
Hoegiro 85, Seoul 02455, Korea*

^b*Center for Geometry and Physics, Institute for Basic Science (IBS),
Pohang 37673, Korea*

E-mail: klee@kias.re.kr, norton.lee@ibs.re.kr

ABSTRACT: We construct dimer graphs for type D relativistic Toda models by introducing impurities to the $Y^{2N,0}$ square dimer graphs. By properly placing the impurities and change of canonical variables assigned to the 1-loops on the dimer graph, we introduce the "folding" of the graphs and get the type D relativistic Toda lattice Hamiltonian and monodromy matrix.

Contents

1	Introduction	2
2	Classical Relativistic Toda of type D	3
2.1	Integrability	4
2.2	RTL with boundary	5
3	Dimer integrable system	7
3.1	Introduce impurities	10
3.2	D_4	11
3.3	D_N	19
4	Lax formalism	20
4.1	Construct Lax matrix from dimer graph	20
4.2	Reconstructing monodromy matrix from double impurity dimer	22
5	Summery and future directions	25
A	Lax formalism	26
A.1	$N \times N$ Lax matrix	26
A.2	2×2 Lax matrix	28
B	Canonical change of variables	29
C	Detail computation in section 4.2	29

1 Introduction

The relativistic Toda lattice (RTLs) was first introduced in [1] with a given Lie algebra \mathfrak{g} . There are two Lax formalism for RTL: The Lax triad which consists three $N \times N$ Lax matrices [2, 3], and Sklyanin's 2×2 r -matrix formalism [4, 5]. Type-A RTL, which defined based on Lie algebra $\mathfrak{g} = A_{N-1}$, belongs to a class of cluster integrable systems proposed by Goncharov and Kenyon [6]: an integrable system in correspondence to a periodic planar dimer placed on a torus [7]. The dual graph of the dimer graph is a planar, periodic quiver. The quiver gauge theory, called $Y^{p,q}$, arises from a stack of D3 branes probing a single, toric Calabi-Yau three-fold (CY3). Both the quiver and the dimer can be constructed based on the toric diagram of the CY3 [8]. Interestingly, recent studies shows that there exist general dimer graphs on top of the "standard" dimer built from the $Y^{p,q}$ quiver [9]. These dimer graphs share the same toric diagram but different conserving Hamiltonians.

A natural question to ask is whether the correspondence between the dimer and RTL can be extended to RTL defined on Lie algebras other than type A. In this note we will focus on the type D RTL defined on affine Lie algebra \hat{D}_N . Our goal is to find the correct dimer graph whose perfect matching reproduces the commuting Hamiltonians of the type D RTL.

It turns out that the connection between relativistic integrable system and five dimensional $\mathcal{N} = 1$ supersymmetric gauge theory proves to be quite useful in the search for the correct dimer graph. The connection between supersymmetric gauge theories and algebraic integrable model, known as *Bethe/Gauge correspondence*, was first observed between four dimensional $\mathcal{N} = 2$ supersymmetric gauge theories and non-relativistic integrable systems. The geometry of the low-energy states of the four dimensional $\mathcal{N} = 2$ supersymmetric gauge theory is identified with the phase space of an algebraic integrable system [10–13]. And the Seiberg-Witten curve of the supersymmetric gauge theory coincides with the spectral curve of the algebraic integrable model. Hence sharing the same toric diagram.

The Bethe/Gauge correspondence can be extended to supersymmetric gauge theory of gauge group G with eight supercharges compactify on a circle of radius r . Its Seiberg-Witten curve corresponds to the spectral curve of the relativistic integrable with $\mathfrak{g} = \text{Lie}(G)$ algebra. The radius $r = \frac{1}{c}$ acts as the inverse of the speed of light. Indeed, the Bethe/Gauge correspondence is how the Seiberg-Witten curve for five dimensional $\mathcal{N} = 1$ theory was constructed [14].

In this note we will focus on finding the correct Dimer graph for the \hat{D}_N RTL. Bethe/Gauge correspondence provides an advantage as the corresponding gauge theory can be embedded into a bigger SU gauge theory then reduce the degree of freedom by folding. In the case of type D, $SO(2N)$ SYM shares the same toric diagram with $SU(2N) + 8F$ gauge theory with eight fundamental hypermultiplets fine-tuned [15]. The O5-plane in the brane construction of $SO(2N)$ gauge group indicates a proper folding from $SU(2N) + 8F$ is required to obtain the correct degree of freedom. This also restrict how the dimer graph should be constructed.

In this note we construct dimer graph based on the type A square dimer with impurities or flavors introduced. By properly placing the impurity and identification of parameters

through folding we successfully construct dimer graph for \hat{D}_N RTL. The monodromy matrix of the type D RTL is constructed from the Kasteleyn matrix of the dimer. Thus recovering all the conserving Hamiltonians.

Outline

This paper is organized as follows: In Section. 2 we give a quick review on the type D RTL and its integrability in the Skyanin's Lax formalism. In Section. 3 we review the construction of square dimer model for type A RTL. We introduce impurity reflecting the modification based on the fundamental matter in the toric diagram $SU(2N)+8F$. We construct the dimer graph that give rise to the correct first \hat{D}_N RTL Hamiltonian after proper folding and change of canonical variables. In Section. 4 we recover Lax/monodromy matrix of \hat{D}_N RTL based on the Kasteleyn matrix of the dimer we constructed.

Finally we point out our conclusion and future direction in Section. 5

Acknowledgments

The authors thank Saebyeok Jeong, Hee-cheol Kim, Minsung Kim, Yongchao Lu, Xin Wang for useful discussion and correspondence. The research of NL is supported by IBS project IBS-R003-D1. KL is supported in part by KIAS Grants PG006904 and the National Research Foundation of Korea (NRF) Grant funded by the Korea government (MSIT) (No. 2017R1D1A1B06034369). KL also thanks KITP for the program [What is String Theory? Weaving Perspectives Together](#). This research was supported in part by grant NSF PHY-2309135 to the Kavli Institute for Theoretical Physics (KITP).

2 Classical Relativistic Toda of type D

The relativistic Toda lattice describes N particles on a line or a ring. The n -th particle's position and momentum are labeled by \mathbf{q}_n and \mathbf{p}_n satisfying the Poisson commutation relation

$$\{\mathbf{q}_n, \mathbf{p}_m\} = \delta_{nm}, \quad n, m = 1, \dots, N. \quad (2.1)$$

Given an Lie algebra \mathfrak{g} , the relativistic Toda lattice (RTL for short) is defined on its simple root system $\mathcal{R}_{\mathfrak{g}}$ [1, 16]. For our interest we will focus on the Toda lattice defined on the affine Lie algebra of type D. The Hamiltonian of relativistic Toda lattice associated to the root system of \hat{D}_N Lie algebra [17, 18]:

$$\mathbb{H}_{\hat{D}_N} = \mathbb{H}_0 + \mathbb{J}_1 + \mathbb{J}_N \quad (2.2)$$

where \mathbb{H}_0 is the open relativistic Toda lattice Hamiltonian of type A:

$$\mathbb{H}_0 = \sum_{n=1}^N 2 \cosh(\mathbf{p}_n) + 2g^2 \sum_{n=1}^{N-1} e^{\mathbf{q}_n - \mathbf{q}_{n+1}} \cosh \frac{\mathbf{p}_n + \mathbf{p}_{n+1}}{2}, \quad (2.3)$$

and

$$\begin{aligned} J_1 &= 2g^2 e^{-\mathfrak{q}_1 - \mathfrak{q}_2} \cosh \frac{\mathfrak{p}_1 - \mathfrak{p}_2}{2} + g^4 e^{-2\mathfrak{q}_2}, \\ J_N &= 2g^2 e^{\mathfrak{q}_N + \mathfrak{q}_{N-1}} \cosh \frac{\mathfrak{p}_N - \mathfrak{p}_{N-1}}{2} + g^4 e^{2\mathfrak{q}_{N-1}}. \end{aligned} \quad (2.4)$$

g is the coupling constant. The total number of terms (written in individual exponential) in the \hat{D}_N RTL Hamiltonian (2.2) is $2N + 2(N - 1) + 3 + 3 = 4N + 4$. One may notice the additional two terms $g^4 e^{-2\mathfrak{q}_2}$ and $g^4 e^{2\mathfrak{q}_{N-1}}$ that do not come from the simple root of \hat{D}_N .

In the non-relativistic limit we scale the coupling $g \rightarrow rg$ and momentum $\mathfrak{p} \rightarrow r\mathfrak{p}$. r is the inverse of the speed of light. The relativistic Hamiltonian can be expand in the powers of r

$$H_{\hat{D}_N} = N + 2r^2 \left[\sum_{n=1}^N \frac{\mathfrak{p}_n^2}{2} + g^2 \sum_{n=1}^{N-1} e^{\mathfrak{q}_n - \mathfrak{q}_{n+1}} + g^2 e^{-\mathfrak{q}_1 - \mathfrak{q}_2} + g^2 e^{\mathfrak{q}_N + \mathfrak{q}_{N-1}} \right] + \mathcal{O}(r^4) \quad (2.5)$$

The coefficient of r^2 in the expansion is exactly the Hamiltonian of type D non-relativistic Toda lattice.

2.1 Integrability

The integrability of RTL is characterized by the R -matrix $R_{a_i, a_j} : V_{a_i} \otimes V_{a_j} \rightarrow V_{a_i} \otimes V_{a_j}$, satisfying the Yang-Baxter equation

$$R_{a_1, a_2}(x - x') R_{a_1, a_3}(x) R_{a_2, a_3}(x') = R_{a_2, a_3}(x') R_{a_1, a_3}(x) R_{a_1, a_2}(x - x'). \quad (2.6)$$

The 2×2 Lax matrix is a special case of the R -matrix with the choice of

$$V_{a_1} = V_{a_2} = \mathbb{C}^2 := V_{\text{aux}}, \quad V_{a_3} = \mathcal{H}$$

on each lattice site. \mathcal{H} is the Hilbert space of a particle. V_{aux} is called the auxiliary space. On each of the lattice site we define a 2×2 Lax operator as a GL_2 -valued function [18–20]

$$L_n(x) = \begin{pmatrix} 2 \sinh \frac{x - \mathfrak{p}_n}{2} & -g e^{-\mathfrak{q}_n} \\ g e^{\mathfrak{q}_n} & 0 \end{pmatrix} \in \text{End}(\mathcal{H}_n \otimes V_{\text{aux}}) \quad (2.7)$$

where $\mathfrak{p}_n = -\hbar \partial_{\mathfrak{q}_n}$ and \mathfrak{q}_n are the canonically conjugated momentum and coordinate of the n -th particle. \mathcal{H}_n is the Hilbert space of the n -th particle and $V_{\text{aux}} = \mathbb{C}^2$ is an auxiliary space. The R -matrix acting on the space $V_{\text{aux}} \otimes V_{\text{aux}}$ by

$$R_{a_1, a_2}(x - x') = \begin{pmatrix} \sinh \frac{x - x' + \hbar}{2} & 0 & 0 & 0 \\ 0 & \sinh \frac{x - x'}{2} & \sinh \frac{\hbar}{2} & 0 \\ 0 & \sinh \frac{\hbar}{2} & \sinh \frac{x - x'}{2} & 0 \\ 0 & 0 & 0 & \sinh \frac{x - x' + \hbar}{2} \end{pmatrix} \quad (2.8)$$

The commutation relations between two elements in the Lax operator is governed by the Yang-Baxter RLL-relation (train track relation)

$$R_{a_1, a_2}(x - x')L_{a_1}(x)L_{a_2}(x') = L_{a_2}(x')L_{a_1}(x)R_{a_1, a_2}(x - x') \quad (2.9)$$

which can be verified true by direct computation.

The monodromy matrix $\mathbf{T}(x)$ of type A RTL (periodic boundary condition) is an ordered product of the Lax matrices across N particles

$$\mathbf{T}(x) = L_N(x)L_{N-1}(x) \cdots L_2(x)L_1(x) \in \text{End} \left(\bigotimes_{n=1}^N \mathcal{H} \otimes V_{\text{aux}} \right) \quad (2.10)$$

It is obvious that the monodromy matrix $\mathbf{T}(x)$ satisfies the same Yang-Baxter equation as the Lax operator:

$$R_{a_1, a_2}(x - x')\mathbf{T}_{a_1}(x)\mathbf{T}_{a_2}(x') = \mathbf{T}_{a_2}(x')\mathbf{T}_{a_1}(x)R_{a_1, a_2}(x - x') \quad (2.11)$$

The spectral curve of the integrable system is defined through introduction of spectral parameter Y :

$$\text{q-det}(\mathbf{T}(x) - Y) = Y^2 - \text{Tr}\mathbf{T}(x)Y + \det \mathbf{T}(x) = 0. \quad (2.12)$$

2.2 RTL with boundary

E. Sklyanin points out that the monodromy matrix of type BCD RTL can be obtained by introducing reflection matrix as boundary condition [4, 17]. The transfer matrix of a RTL with boundary condition is given by

$$\mathbf{T}(x) = \text{Tr}K_+(x)\mathbf{t}(x)K_-(x)\mathbf{t}^{-1}(-x) \quad (2.13)$$

$\mathbf{t}(x) \in \text{End} \left(\bigotimes_{n=1}^N \mathcal{H} \otimes V_{\text{aux}} \right)$ is the monodromy matrix of the type A RTL. $K_{\pm}(x) \in \text{End}(V_{\text{aux}})$ are the reflection matrices obeying the reflection equation

$$\begin{aligned} R_{12}(x - x')K_{-,1}(x)R_{21}(x + x' - \hbar)K_{-,2}(x') \\ = K_{-,2}(x')R_{12}(x + x' - \hbar)K_{-,1}(x)R_{21}(x - x') \end{aligned} \quad (2.14)$$

and

$$\begin{aligned} R_{12}(-x + x')K_{-,1}^T(x)R_{21}(-x - x' - \hbar)K_{-,2}^T(x') \\ = K_{+,2}^T(x')R_{12}(-x - x' - \hbar)K_{+,1}^T(x)R_{21}(-x + x') \end{aligned} \quad (2.15)$$

Given a simple solution $K_{\pm}(x)$ to the reflection equation, one can check that

$$U_+^T(x) = \mathbf{t}_+^T(x)K_+^T(x)(\mathbf{t}_+^{-1}(-x))^T \quad (2.16a)$$

$$U_-(x) = \mathbf{t}_-(x)K_-(x)\mathbf{t}_-^{-1}(-x) \quad (2.16b)$$

satisfy the same reflection equation if $\mathbf{T}_\pm(x)$ satisfy (2.11). The transfer matrix (trace of monodromy matrix) is the generating function of the integral of motion:

$$\begin{aligned} T(x) &= \text{Tr } U_+ U_- = \text{Tr } K_+(x) \mathbf{t}(x) K_-(x) \mathbf{t}(-x)^{-1} \\ &= e^{\frac{N}{2}x} \left[1 + \sum_{n=1}^N H_n e^{-nx} \right] \end{aligned} \quad (2.17)$$

The reflection matrices K_\pm satisfying the reflection equation takes the following form:

$$K_+(\mathbf{q}_1, \mathbf{p}_1) = \begin{pmatrix} \alpha_1^+ e^{\frac{x}{2}} - \alpha_2^+ e^{-\frac{x}{2}} & \delta^+(e^x + e^{-x}) - \beta^+ \\ \gamma^+ - \delta^+(e^x + e^{-x}) & \alpha_2^+ e^{\frac{x}{2}} - \alpha_1^+ e^{-\frac{x}{2}} \end{pmatrix} \quad (2.18a)$$

$$K_-(\mathbf{q}_N, \mathbf{p}_N) = \begin{pmatrix} -\alpha_1^- e^{\frac{x}{2}} + \alpha_2^- e^{-\frac{x}{2}} & \gamma^- - \delta^-(e^x + e^{-x}) \\ \delta^-(e^x + e^{-x}) - \beta^- & -\alpha_2^- e^{\frac{x}{2}} + \alpha_1^- e^{-\frac{x}{2}} \end{pmatrix} \quad (2.18b)$$

which gives the first Hamiltonian:

$$\begin{aligned} H_1 &= \sum_{j=2}^{N-1} 2 \cosh \mathbf{p}_j + \sum_{j=2}^{N-2} g^2 e^{\mathbf{q}_j - \mathbf{q}_{j+1}} 2 \cosh \frac{\mathbf{p}_j + \mathbf{p}_{j+1}}{2} \\ &+ \beta^+ + \beta^- + g \alpha_1^+ e^{-\frac{\mathbf{p}_2}{2} - \mathbf{q}_2} + g \alpha_2^+ e^{\frac{\mathbf{p}_2}{2} - \mathbf{q}_2} + g \alpha_1^- e^{-\frac{\mathbf{p}_{N-1}}{2} + \mathbf{q}_{N-1}} + g \alpha_2^- e^{\frac{\mathbf{p}_{N-1}}{2} + \mathbf{q}_{N-1}} \\ &+ \delta^+ g^2 e^{-2\mathbf{q}_2} + \delta^- g^2 e^{2\mathbf{q}_{N-1}}. \end{aligned} \quad (2.19)$$

The boundary reflection matrices K_\pm for the RTL of type D [18] are:

$$K_+ = \begin{pmatrix} g[e^{\frac{x}{2}} 2 \cosh(\mathbf{p}_1/2 - \mathbf{q}_1) - e^{-\frac{x}{2}} 2 \cosh(\mathbf{p}_1/2 + \mathbf{q}_1)] & 2 \cosh x - 2 \cosh \mathbf{p}_1 \\ g^2[2 \cosh 2\mathbf{q}_1 - 2 \cosh x] & g[e^{-\frac{x}{2}} \cosh(\mathbf{p}_1/2 - \mathbf{q}_1) - e^{\frac{x}{2}} \cosh(\mathbf{p}_1/2 + \mathbf{q}_1)] \end{pmatrix} \quad (2.20a)$$

$$K_- = \begin{pmatrix} g[e^{-\frac{x}{2}} \cosh(\mathbf{p}_N/2 - \mathbf{q}_N) - e^{\frac{x}{2}} \cosh(\mathbf{p}_N/2 + \mathbf{q}_N)] & g^2[2 \cosh 2\mathbf{q}_N - \cosh x] \\ 2 \cosh x - 2 \cosh \mathbf{p}_N & g^2[e^{\frac{x}{2}} \cosh(\mathbf{p}_N/2 - \mathbf{q}_N) - e^{-\frac{x}{2}} \cosh(\mathbf{p}_N/2 + \mathbf{q}_N)] \end{pmatrix} \quad (2.20b)$$

The monodromy matrix $\mathbf{T}(x)$ of \hat{D}_N RTL is

$$\mathbf{T}(x) = K_+(x) \tilde{L}_2(x) \cdots \tilde{L}_{N-1}(x) K_-(x) L_{N-1}(x) \cdots L_2(x). \quad (2.21)$$

with

$$\tilde{L}_n(x) = \begin{pmatrix} 0 & -g e^{-\mathbf{q}_n} \\ g e^{\mathbf{q}_n} & 2 \sinh \frac{x + \mathbf{p}_n}{2} \end{pmatrix} = g^4 L_n^{-1}(-x). \quad (2.22)$$

The spectral curve of classical integrable system is defined by ¹

$$0 = \det(\mathbf{T}(x) - Y) = Y^2 - \text{Tr} \mathbf{T}(x) Y + \det \mathbf{T}(x) \quad (2.23)$$

¹The determinant is replaced by q-determinant when quantizing the integrable system.

The determinant of the monodromy matrix $t(x)$ is nothing but the product of the determinant of its individual building blocks:

$$\det \mathbf{T}(x) = g^{4N-8} (X - X^{-1})^4, \quad X = e^x.$$

We scale $Y \rightarrow Y g^{2N-4} (X - X^{-1})^2$ to obtain the spectral curve:

$$g^{2N-4} (X - X^{-1})^2 Y - T(X) + g^{2N-4} \frac{(X - X^{-1})}{Y} = 0. \quad (2.24)$$

Type D relativistic Toda is applied to the description of SW ansatz for $SO(2N)$ pure gauge theory [21]. The Seiberg-Witten curve for 5d $\mathcal{N} = 1$ $SO(2N)$ pure SYM is

$$(X - X^{-1})^2 Y + 2 \prod_{\alpha=1}^N (X U_{\alpha} - X^{-1} U_{\alpha}^{-1}) (X U_{\alpha}^{-1} - X^{-1} U_{\alpha}) + \frac{(X - X^{-1})^2}{Y} = 0 \quad (2.25)$$

The corresponding toric diagram \mathcal{T} can be obtained from the D-brane/O-plane construction. See Fig. 1 for illustration.

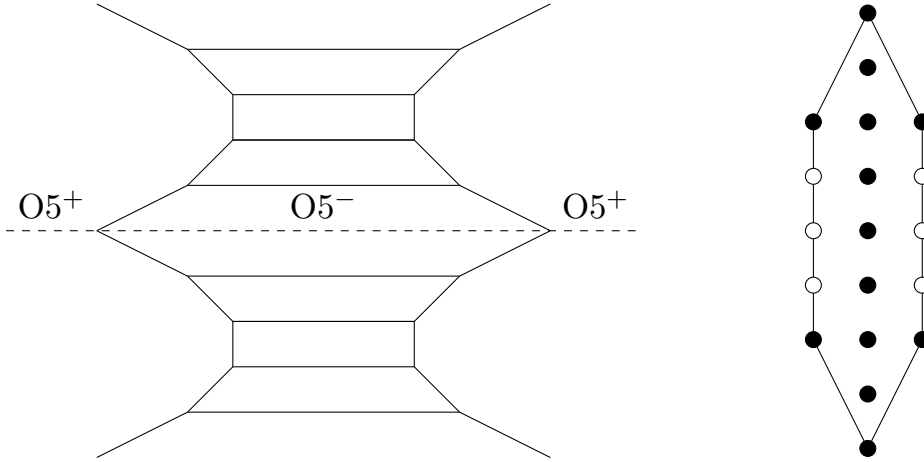


Figure 1. The brane construction of $SO(8)$ gauge group with toric nodes indicated by the brane construction. Notice that $O5^+$ branes are replaced by 3 nodes instead of 1. See [15] for detail.

3 Dimer integrable system

Relativistic Toda system belongs to a class of cluster integrable model discovered by [6]. A way to construct them is through the *dimer model*, also known as *brane tiling*. It is proven in [6] that any dimer model on a torus defines an relativistic integrable model.

A bipartite graph $\Gamma = (B, W, E)$ embedded on a oriented 2-manifold \mathcal{S} consists

- a finite set $B \subset \mathcal{S}$ of black nodes,
- a finite set $W \subset \mathcal{S}$ of white nodes, and

- a finite set E of edges, consisting of embedded closed intervals e on \mathcal{S} such that one boundary of e belongs to B and the other boundary belongs to W ,

such that any edge can intersect another edge only at its boundary [22]. A bipartite graph $\Gamma = (B, W, E)$ is a dimer model if the following two conditions are satisfied:

- Every equivalent node is on the boundary of \mathcal{S} , and
- every faces of Γ is simply-connected.

In this note we will consider the case $\mathcal{S} = T^2$. When placed on the torus, a dimer is characterized by a *unit cell* with periodicity on both the horizontal and vertical direction of the unit cell boundary. The boundary of the unit cell corresponds to the two cycles of the torus.

The dual graph of the dimer graph is a planar, periodic quiver [23]. Quiver gauge theories described by dimer graphs arise from the worldvolume of a stack of D3-branes probing a single Calabi-Yau (CY) 3-fold. The connection between dimer models and quivers has trivialized the determination of the Calabi-Yau geometry [23–25].

Given a bipartite graph $\Gamma = (B, W, E)$, a perfect matching $\mathbb{M} \subset E$ is a collection of edges $e \in E$ such that all nodes (black and white) in Γ are connected by exactly one edge. We choose the default orientation of the edges to be pointing from a black node to a white node, such that given a perfect matching \mathbb{M} , we define $-\mathbb{M}$ as the same collection of the edges but with opposite orientation (white to black). We assign to each oriented edge a weight w_e :

$$w_e = \begin{cases} X, & \text{The edge cross vertical boundary with positive orientation.} \\ X^{-1}, & \text{The edge cross vertical boundary with negative orientation.} \\ Y, & \text{The edge cross horizontal boundary with positive orientation.} \\ Y^{-1}, & \text{The edge cross horizontal boundary with negative orientation.} \\ 1, & \text{The edge lies within the unit cell.} \end{cases} \quad (3.1)$$

The weight of a perfect matching \mathbb{M} is a product over the weight of all its edges:

$$W[\mathbb{M}] = \prod_{e \in \mathbb{M}} w_e \quad (3.2)$$

The curve of the dimer graph Γ is the ensemble of all possible perfect matchings' weight:

$$W(X, Y) = \sum_{\{\mathbb{M}\}} W[\mathbb{M}] \quad (3.3)$$

This curve happens to be the mirror curve of the Calabi-Yau 3-fold. It can also be obtained by considering the *Kasteleyn matrix* of the dimer [26]. The Kasteleyn matrix is a weighted adjacency matrix of the graph. A toric diagram \mathcal{T} can be associated to the dimer graph Γ based on its curve $W(X, Y)$ [8].

A class of cluster integrable systems for the dimer graphs are proposed in [6]. The integrable system is realized based on the *loops* on the dimer. A 1-loop is a path connecting

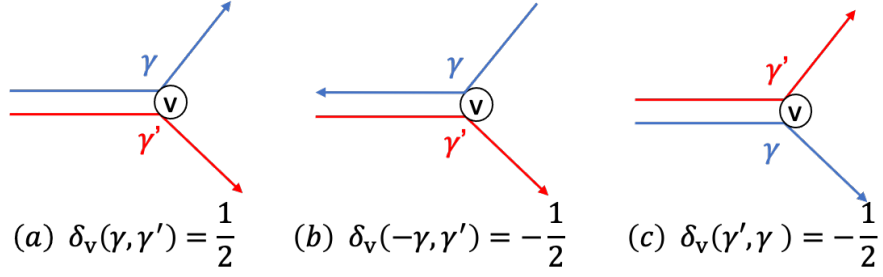


Figure 2. An illustration of $\delta_v(\gamma, \gamma')$.

from a node to the same node in the next unit cell. We choose one perfect matching as the reference perfect matching \mathbb{M}_{ref} . In this note we always choose the perfect matching that corresponds to the furthest point in the positive X axis on the corresponding toric diagram \mathcal{T} . The 1-loops can be systematically constructed by subtracting a perfect matching from the reference perfect matching $\mathbb{M} - \mathbb{M}_{\text{ref}}$.

Following [8, 22], the commutation relation and Hamiltonians of the cluster integrable system can be read off from the loops on the graph. Let γ and γ' be two oriented loops on the dimer graph Γ . The Poisson commutation relation between the loops are defined as

$$\{\gamma, \gamma'\} = \epsilon_{\gamma\gamma'} \gamma\gamma' \quad (3.4)$$

where

$$\{\gamma, \gamma'\} = \sum_v \text{sgn}(v) \delta_v(\gamma, \gamma') \quad (3.5)$$

Here $\text{sgn}(v) = 1$ for the black node and $\text{sgn}(v) = -1$ for the white node. δ_v is a skewsymmetric bilinear form satisfying

$$\delta_v(\gamma, \gamma') = -\delta_v(\gamma', \gamma) = -\delta_v(-\gamma, \gamma') \in \frac{1}{2}\mathbb{Z}$$

as illustrated in Fig. 2.

The n -loop is defined as product of n non-overlapping 1-loops. The n -th Hamiltonian of the dimer integrable system is given by the ensemble over all the n -loops.

The dimer model associated to the type A RTL is known as $Y^{N,0}$ model constructed by periodic square diagrams. The shape of the unit cell depends on whether N is even (rectangular) or odd (rhombus). For the purpose of this paper, here we consider the case N being even. Each unit cell consists two columns of N squares along with N white and black vertices $\mathbf{w}_n, \mathbf{b}_n, n = 1, \dots, N$. See Figure. 3 for illustration.

The first Hamiltonian of the $Y^{N,0}$ dimer coincide with the \hat{A}_{N-1} RTL Hamiltonian once the 1-loops are expressed in terms of the canonical coordinates. The Lax matrix of \hat{A}_{N-1} RTL can be constructed from the Kasteleyn matrix. We will not get in to the detail here but refer the interested reader to Appendix. A and [7, 9] for more detail.

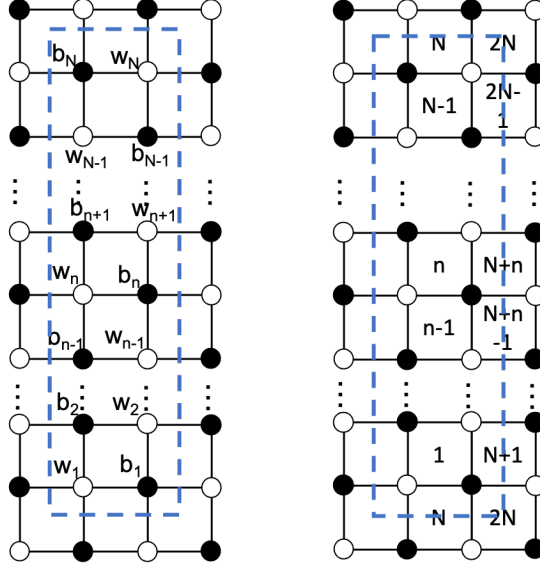


Figure 3. The brane tiling for $Y^{N,0}$ dimer model with N even. A unit cell is encircled by the dashed blue line. This dimer is associated to the \hat{A}_{N-1} relativistic Toda lattice.

3.1 Introduce impurities

The relation between the toric diagram and dimer graph works in both direction. A dimer graph $\Gamma = (B, W, E)$ can be constructed based on a given toric diagram \mathcal{T} [7, 8]. In some cases multiple dimer graphs can be constructed based on a single toric diagram [9].

We use the following two facts to construct the dimer model for \hat{D}_N :

- SW curve of Super Young-Mills theory of gauge group G coincide with spectral curve of RTL of Lie algebra $\mathfrak{g} = \text{Lie}(G)$.
- $SO(2N)$ gauge theory shares the same toric diagram with $SU(2N)$ gauge theory with 8 fundamental matters fine-tuned, and can be embedded into $SU(2N)$ theory with folding to reduce the degree of freedom.

The dimer graph associated to the toric diagram for $SU(2N) + 8F$ can be constructed by introducing impurity in the $Y^{2N-4,0}$ model (A_{2N-4} RTL). This is indicated by the slopes of the four long edges of the toric diagram. The D_N dimer then can be obtained through the process of folding by eliminating the degrees of freedom by half.

The 8 short vertical lines in the toric diagram \mathcal{T} introduce impurity to the square dimer in the following way: When $N \geq 4$, we pick 4 among $2N - 4$ squares in the unit cell the n_i -th square, $i = 1, 2, 3, 4$, $n_i \in \{1, \dots, 2N - 4\}$, to introduce impurity. Two pairs of black and white nodes, which we will denote by $\tilde{\mathbf{w}}_{n_i}^{(1,2)}$ and $\tilde{\mathbf{b}}_{n_i}^{(1,2)}$ are added in the middle of the n_i -th square in the order white-black-white-black starting from the left of the unit cell. The vertical edges of n_i -th squares are removed and replaced by

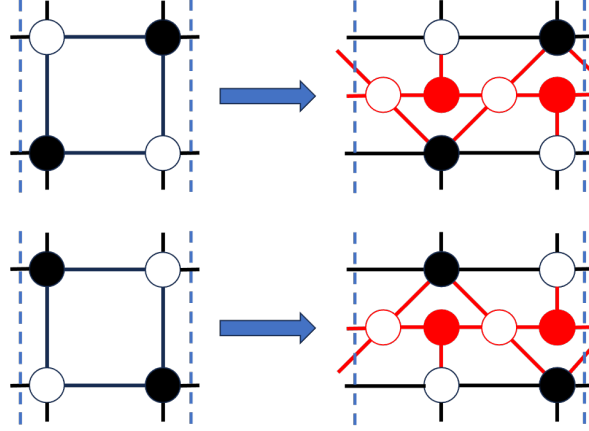


Figure 4. The vertical lines in the toric diagram \mathcal{J} introduces impurity to the square dimer graph. The newly introduced red nodes modifies the edges inside the square. The boundary of the unit cell is indicated by blue dashed lines.

- Horizontal lines connecting the newly introduced black and white nodes, which also extended to outside of the the unit cell.
- Two vertical lines connecting the newly introduced black nodes $\mathbf{b}_{n_i}^{(l)}$, $l = 1, 2$ to the square's white nodes $\mathbf{w}_{n_i - \frac{1}{2} + \frac{(-1)^{n_i}}{2}}$.
- Two slide edges connecting $\mathbf{w}_{n_i}^l$, $l = 1, 2$, to \mathbf{b}_{n_i} and \mathbf{b}_{n_i-1} .

See Fig. 4 for illustration.

There is a different way to introduce defect to the A_{2N-4} dimer by place double impurity to a single square. Four pairs of white and black nodes are added to the middle of the square. See Fig. 5 for illustration.

The final dimer graph will have exactly $2N - 4 + 4 \times 2 = 2N + 4$ pairs of black and white nodes distributed on exactly $2N$ rows.

3.2 D_4

The dimer graph for D_4 system can be constructed by introducing impurity to A_4 dimer. The impurity can be introduced in the form of 4 single or 2 double,. Fig. 6 illustrate two different bipartite graph. More general cases can be considered, which we will leave the discussion in the furture.

The Kastelyne matrix $K_{4,D}$ of the double impurity bipartite graph in Fig. 6 is:

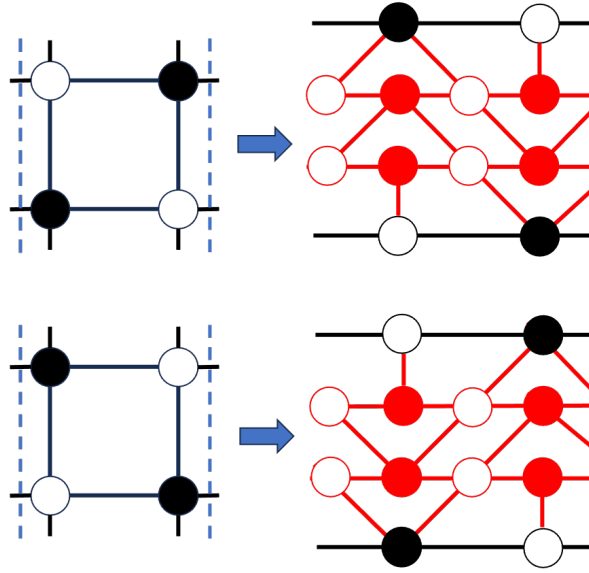


Figure 5. The vertical lines in the toric diagram \mathcal{T} introduces double impurity to the square dimer graph. The newly introduced red nodes modifies the edges inside the square. The boundary of the unit cell is indicated by blue dashed lines.

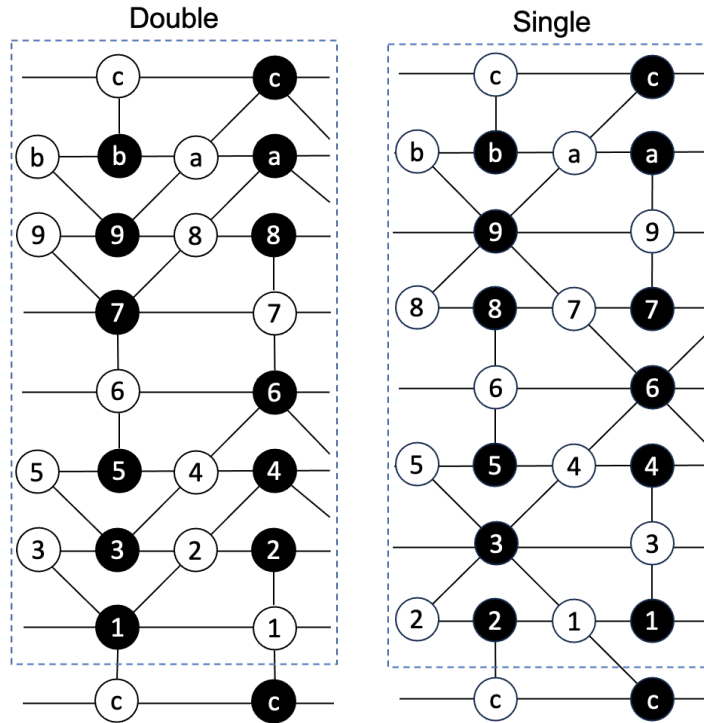


Figure 6. Two bipartite graphs generated by toric diagram for $D_4/A_7 + 8F$ in Fig. 1. The left graph is constructed by placing double impurity at the first and third square in A_4 graph. The right one place single impurity in each of the square in the A_4 graph.

	1	2	3	4	5	6	7	8	9	a	b	c
1	$h_{1r} - \frac{h_{1l}}{X}$	s_{12}	s_{13}	0	0	0	0	0	0	0	0	$\frac{v_{1c}}{Y}$
2	v_{21}	$-h_2$	$h_{23}X$	0	0	0	0	0	0	0	0	0
3	0	h_{32}	$-h_3$	s_{34}	s_{35}	0	0	0	0	0	0	0
4	0	s_{42}	$s_{43}X$	$-h_4$	$h_{45}X$	0	0	0	0	0	0	0
5	0	0	0	h_{54}	$-h_5$	v_{56}	0	0	0	0	0	0
6	0	0	0	s_{64}	$s_{65}X$	$h_{6r}X - h_{6l}$	v_{67}	0	0	0	0	0
7	0	0	0	0	0	v_{76}	$h_{7r} - \frac{h_{7l}}{X}$	s_{78}	s_{79}	0	0	0
8	0	0	0	0	0	0	v_{87}	$-h_8$	$h_{89}X$	0	0	0
9	0	0	0	0	0	0	0	h_{98}	$-h_9$	s_{9a}	h_{9b}	0
a	0	0	0	0	0	0	0	s_{a8}	$s_{a9}X$	$-h_a$	$h_{ab}X$	0
b	0	0	0	0	0	0	0	0	0	h_{ba}	$-h_b$	v_{bc}
c	$v_{c1}Y$	0	0	0	0	0	0	0	0	s_{ca}	$s_{cb}X$	$h_{cr}X -$

In particular, when setting all parameter (beside x and y) to 1 gives

$$\begin{aligned} \frac{\det K_{4,D}}{x^2} = & X^4 + \frac{1}{X^4} - 36 \left(X^3 + \frac{1}{X^3} \right) + 406 \left(X^2 + \frac{1}{X^2} \right) - 1556 \left(X + \frac{1}{X} \right) + 2402 \\ & - \left(Y + \frac{1}{Y} \right) \left(X^2 - 4X + 6 - \frac{4}{X} + \frac{1}{X^2} \right) \end{aligned} \quad (3.6)$$

We choose the reference perfect matching that each dimer covers $\mathbf{w}_i \rightarrow \mathbf{b}_i$ with all arrows going rightward. The number of 1-loops is the coefficient of $-x^3$ in (3.6): 36. These 1-loops are distributed across the 8 horizontal lines:

- Lines with \mathbf{w}_1 and \mathbf{w}_7 : 7 in total;
- Lines with \mathbf{w}_3 and \mathbf{w}_9 : 7 in total;
- Lines with \mathbf{w}_5 and \mathbf{w}_b : 3 in total;
- Lines with \mathbf{w}_6 and \mathbf{w}_c : 1 in total;

See Fig. 7 for illustration of the 1-loops. Most of the 1-loops can be build from straight lines d_j , $j = 1, 2, 3, 4$, and square loops S_n , $n = 1, \dots, 7$. See Fig. 8 for illustration.

The double impurity dimer is constructed from the $A_7 + 8F$ toric diagram Fig.1. The masses m_f , $f = 1, \dots, 8$ are fine-tuned to

$$m_1 = m_2 = 0, \quad m_3 = -m_4 = -i\pi, \quad m_5 = m_6 = 0, \quad m_7 = -m_8 = -i\pi. \quad (3.7)$$

The first Hamiltonian for the double impurity (the dimer graph on the left of Fig. 6 is

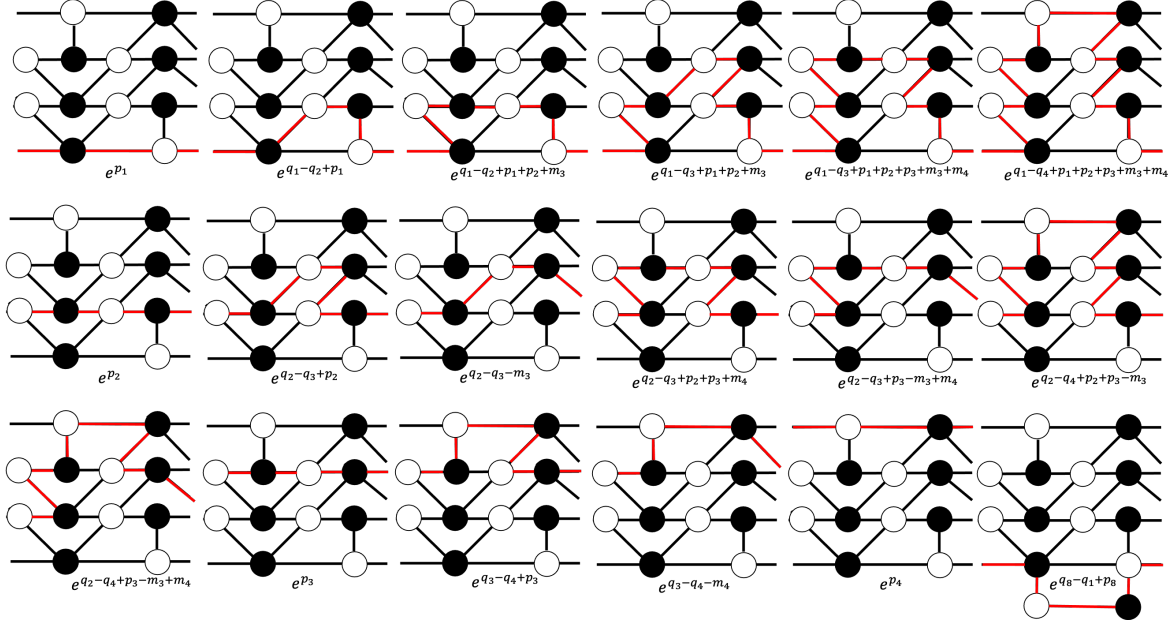


Figure 7. 18 1-loops in the double impurity $SU(8) + 8F$ dimer graph.

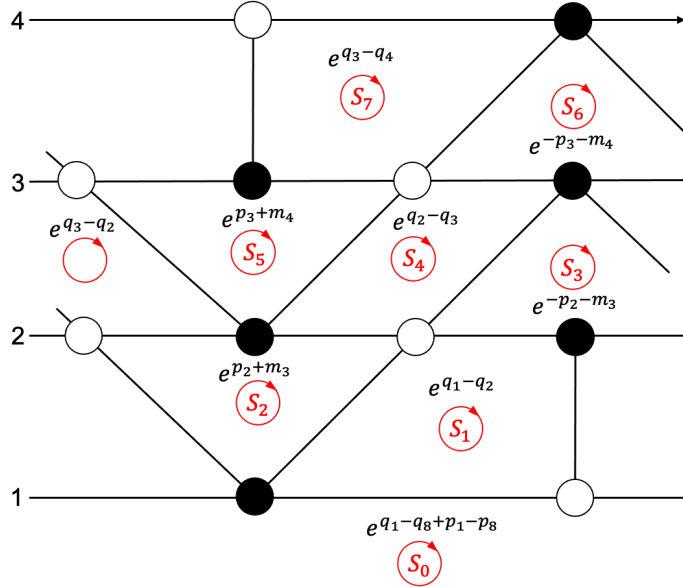


Figure 8. Basic square loops in the modified unit cell in double impurity dimer. The four masses are encoded in the dimer graph through the square loops and impurity straight lines.

the sum over all 1-loops:

$$\begin{aligned}
H_1 = & e^{P_1} \left[1 + e^{q_1 - q_2} - e^{q_1 - q_2 + p_2} - e^{q_1 - q_3 + p_2} + e^{q_1 - q_3 + p_2 + p_3} + e^{q_1 - q_4 + p_2 + p_3} \right] \\
& + e^{P_2} \left[1 + e^{q_2 - q_3} - e^{q_2 - q_3 - p_2} - e^{q_2 - q_3 + p_3} + e^{q_2 - q_3 - p_2 + p_3} - e^{q_2 - q_4 + p_3} + e^{q_2 - q_4 - p_2 + p_3} \right] \\
& + e^{P_3} \left[1 + e^{q_3 - q_4} - e^{q_3 - q_4 - p_3} \right] \\
& + e^{P_4} \left[1 + e^{q_4 - q_5} \right] \\
& + e^{P_5} \left[1 + e^{q_5 - q_6} - e^{q_5 - q_6 + p_6} - e^{q_5 - q_7 + p_6} + e^{q_5 - q_7 + p_6 + p_7} + e^{q_5 - q_8 + p_6 + p_7} \right] \\
& + e^{P_6} \left[1 + e^{q_6 - q_7} - e^{q_6 - q_7 - p_6} - e^{q_6 - q_7 + p_7} + e^{q_6 - q_7 - p_6 + p_7} - e^{q_6 - q_8 + p_7} + e^{q_6 - q_8 - p_6 + p_7} \right] \\
& + e^{P_7} \left[1 + e^{q_7 - q_8} - e^{q_7 - q_8 - p_7} \right] \\
& + e^{P_8} \left[1 + e^{q_8 - q_1} \right]
\end{aligned} \tag{3.8}$$

The 7th Hamiltonian is the sum over all 7-loops, which are product of seven non-overlapping 1-loops. It also consists 36 terms.

$$\begin{aligned}
e^{-P_{\text{tot}}} H_7 = & e^{-P_1} \left[1 + e^{q_8 - q_1} \right] \\
& + e^{-P_2} \left[1 + e^{q_1 - q_2} - e^{q_1 - q_2 + p_2} \right] \\
& + e^{-P_3} \left[1 + e^{q_2 - q_3} - e^{q_2 - q_3 - p_2} - e^{q_2 - q_3 + p_3} + e^{q_2 - q_3 - p_2 + p_3} - e^{q_1 - q_3 - p_2} + e^{q_1 - q_3 - p_2 + p_3} \right] \\
& + e^{-P_4} \left[1 + e^{q_3 - q_4} - e^{q_3 - q_4 - p_3} - e^{q_2 - q_4 - p_3} + e^{q_2 - q_4 - p_3 - p_2} + e^{q_1 - q_4 - p_3 - p_2} \right] \\
& + e^{-P_5} \left[1 + e^{q_4 - q_5} \right] \\
& + e^{-P_6} \left[1 + e^{q_5 - q_6} - e^{q_5 - q_6 + p_6} \right] \\
& + e^{-P_7} \left[1 + e^{q_6 - q_7} - e^{q_6 - q_7 - p_6} - e^{q_6 - q_7 + p_7} + e^{q_6 - q_7 - p_6 + p_7} - e^{q_5 - q_7 - p_6} + e^{q_5 - q_7 - p_6 + p_7} \right] \\
& + e^{-P_8} \left[1 + e^{q_7 - q_8} - e^{q_7 - q_8 - p_7} - e^{q_6 - q_8 - p_7} + e^{q_6 - q_8 - p_7 - p_6} + e^{q_5 - q_8 - p_7 - p_6} \right]
\end{aligned} \tag{3.9}$$

Indeed it consists 36 terms.

We want to match $H_1 = H_7$ to fold $SU(8) + 8F$ to $SO(8)$. The solution is

$$\begin{aligned}
q_1 = -q_4, \quad p_1 = -p_4, \quad q_2 = -q_3, \quad p_2 = -p_3 \\
q_5 = -q_8, \quad p_5 = -q_8, \quad q_6 = -q_7, \quad p_6 = -p_7
\end{aligned} \tag{3.10}$$

Imposing the solution to the first Hamiltonian:

$$\begin{aligned}
H_1 = & 2 \cosh p_1 + 2 \cosh p_2 + 2 \cosh p_7 + 2 \cosh p_8 \\
& + e^{q_1 - q_2} (e^{p_1} + e^{-p_2} - 1 - e^{p_1 + p_2}) \\
& + e^{q_7 - q_8} (e^{p_7} + e^{-p_8} - 1 - e^{-p_7 - p_8}) \\
& + e^{q_8 - q_1} (e^{-p_1} + e^{p_8}) \\
& + e^{q_1 + q_2} (e^{p_1} + e^{-p_2} - 1 - e^{p_1 + p_2}) \\
& + e^{-q_7 - q_8} (e^{p_7} + e^{-p_8} - 1 - e^{-p_7 - p_8}) \\
& + e^{2q_1 + p_1} + e^{2q_2} [e^{p_2} - 2 + e^{-p_2}] + e^{-2p_7} [e^{p_7} - 2 + e^{-p_7}] + e^{-2q_8 - p_8}
\end{aligned} \tag{3.11}$$

We would like to point out that the identification (3.10) causes the Poisson commutation relation defined for shared edges potentially failed when there are square loops between the double impurity line (S_3 , S_4 , and S_5 in Fig. 8). After the imposing the solution, the Poisson commutation relation involves S_4 are doubled despite sharing only one edge:

$$\frac{\{S_4, S_2\}}{S_4 S_2} = \frac{\{S_5, S_4\}}{S_5 S_4} = \frac{\{S_3, S_4\}}{S_3 S_4} = \frac{\{S_4, S_6\}}{S_4 S_6} = \frac{\{S_4, e^{p_2}\}}{S_4 e^{p_2}} = 2.$$

Follow by $q_1 \rightarrow q_1 - \frac{p_1}{2}$, $q_8 \rightarrow q_8 - \frac{p_8}{2}$ and

$$e^{q_2} \rightarrow \frac{\cosh \frac{p_2}{2}}{\sinh \frac{q_2}{2}}, \quad e^{p_2} \rightarrow \frac{\cosh \frac{p_2 - 2q_2}{2}}{\cosh \frac{p_2 + 2q_2}{2}}; \quad e^{q_7} \rightarrow \frac{\sinh \frac{q_7}{2}}{\cosh \frac{p_7}{2}}, \quad e^{p_7} \rightarrow \frac{\cosh \frac{p_7 + 2q_7}{2}}{\cosh \frac{p_7 - 2q_7}{2}} \tag{3.12}$$

This change of variable is canonical, i.e. preserves the Poisson commutation relation. This can be checked by direct computation. See Appendix. B for computational detail. Finally we modify $S_{1,7}$ by

$$S_1 \rightarrow S_1 \frac{\cosh \frac{p_2}{2}}{\sinh \frac{p_2}{2}}, \quad S_7 \rightarrow S_7 \frac{\sinh \frac{p_2}{2}}{\cosh \frac{p_2}{2}}. \tag{3.13}$$

The same modification is also applied to the other double impurity. The first Hamilton H_1 after the change of canonical coordinate becomes:

$$\begin{aligned}
H_1 = & 2 \cosh p_1 + 2 \cosh p_2 + 2 \cosh p_7 + 2 \cosh p_8 \\
& + e^{q_1 - q_2} 2 \cosh \frac{p_1 + p_2}{2} + e^{q_8 - q_1} 2 \cosh \frac{p_8 + p_1}{2} + e^{q_7 - q_8} 2 \cosh \frac{p_7 + p_8}{2} \\
& + e^{q_1 + q_2} 2 \cosh \frac{p_1 - p_2}{2} + e^{-q_7 - q_8} 2 \cosh \frac{p_7 - p_8}{2} + e^{2q_1} + e^{-2q_8}
\end{aligned} \tag{3.14}$$

After renaming $1 \rightarrow 3$, $2 \rightarrow 4$, $8 \rightarrow 2$, and $7 \rightarrow 1$, we recover (2.2) with coupling $g = 1$

$$H_1 = H_{D_4}.$$

On the double impurity dimer graph, we identify the vertexes and faces in the double impurity $SU(8) + 8F$ dimer graph according to the solution (3.10). The unit cell with (3.10)

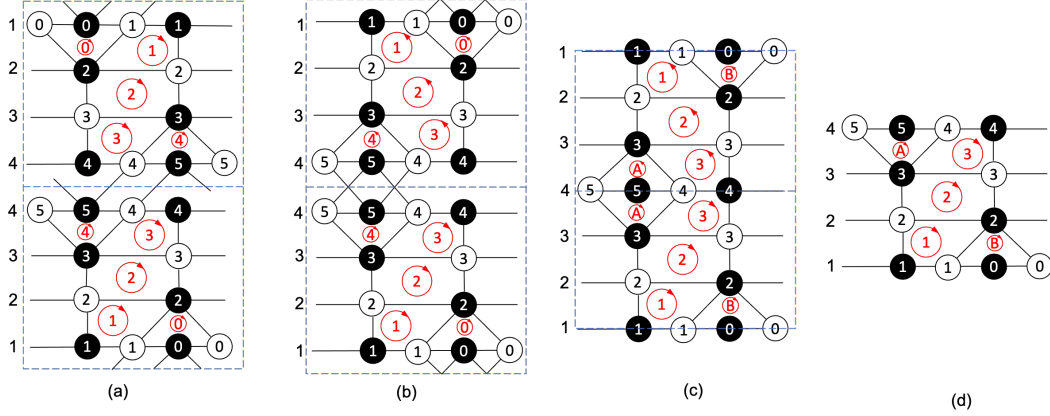


Figure 9. Identifying the vertexes and faces in the double impurity dimer Fig. 8 based on Eq. (3.10) in figure (a). In (b) the top half unit cell is reflected horizontally. The change of canonical coordinate (3.12) modifies the two 1st and two 4th line. This further allows folding of the top half unit cell to obtain (d).

can be composed by two identical half unit cell with one rotated by 180 degree and placed on the bottom of the other one (the identification is based on the level of the square loop). This identification across two half unit cell allows folding. The edges across the half unit cell connecting a node A in one half unit cell and a node B in another unit cell are removed according to the change of variable (3.12). See Fig. 9 for illustration. This modification further modified the Poisson commutation relation between the 1-loops sharing the double edges.

We obtain the dimer graph in Fig. 10. To construct the 1-loop, we choose the perfect matching on the D_4 dimer to be horizontal edges that has white node on the left of the black node. There are 9 1-loops based on such reference matching. Next we rotate the dimer graph with the 1-loop by 180 degree. This gives another 9 1-loops on the folded patch. Notice that the rotation by 180 degree is equivalent to have a different reference perfect matching with the white nodes on the right of the black nodes on each horizontal edge.

We assign the faces loops in the D_4 dimer to obey the Poisson commutation relation based on the shared edges and horizontal 1-loops in Fig. 10, which is enough to determine all $9 + 9 = 18$ 1-loops in Fig. 11:

The first Hamiltonian of dimer graph Fig. 10 is the sum over all 1-loops plus the two additional terms coming from connecting the two patches (top right of Fig. 7):

$$\begin{aligned}
H_1 = & 2 \cosh p_1 + 2 \cosh p_2 + 2 \cosh p_3 + 2 \cosh p_4 \\
& + e^{q_1 - q_2} (1 + e^{p_1 + p_2}) + e^{q_2 - q_3} (e^{p_3} + e^{-p_2}) + e^{p_3 - p_4} (e^{p_4} + e^{p_3}) \\
& + e^{-q_1 - q_2} (e^{-p_1} + e^{p_2}) + e^{q_3 + q_4} (e^{p_4} + e^{p_3}) + e^{-2q_2} + e^{2q_3}
\end{aligned} \tag{3.15}$$

Change the canonical coordinate by

$$q_{2,3} = q_{2,3} + \frac{p_{2,3}}{2}, \quad q_{1,4} = q_{1,4} - \frac{p_{1,4}}{2}$$

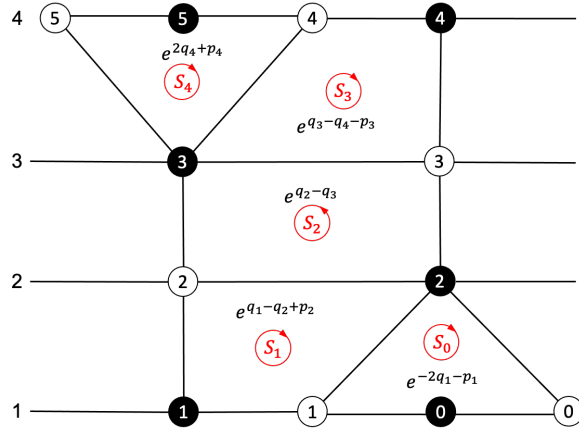


Figure 10. Half of dimer graph for D_4 theory, obtained from folding $SU(8)+8F$ with double impurity Fig. 6. The full dimer is two copies of the half-dimer, with the second rotated by 180 degree.

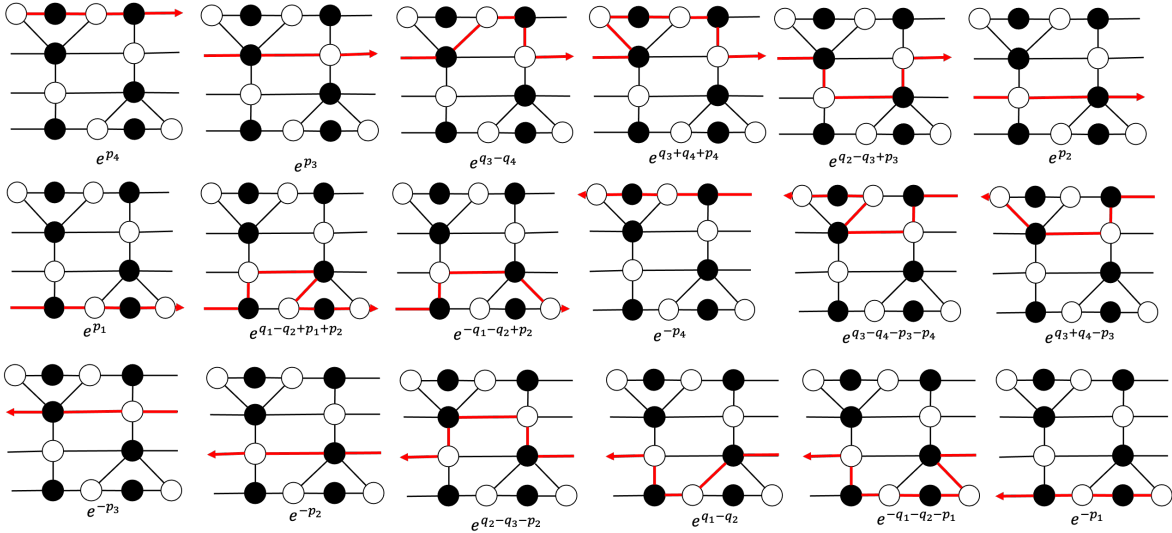


Figure 11. 18 1-loops in the D_4 dimer graph. The 6 in the top line and the left 3 on the middle are obtained by the reference perfect matching. The other 9 (right 3 in the middle and bottom 6) are obtained via rotating the dimer by 180 degree/alternative perfect matching. There are two more 1-loops coming from connecting between two half unit cell.

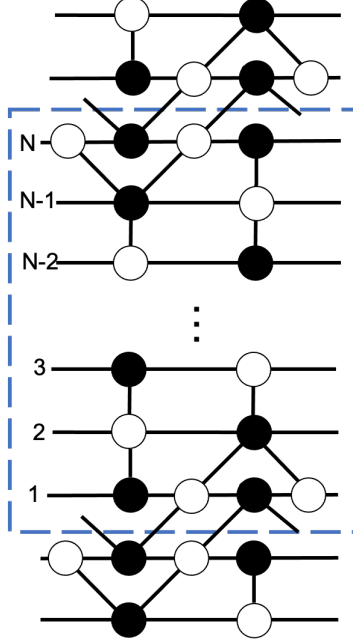


Figure 12. A proposed bipartite graphs to be folded to dimer for D_N system with even N . The blue dashed square labels HALF unit cell in $U(2N) + 8F$ dimer, which would become the dimer for D_N .

and we identify the first Hamiltonian as the D_4 relativistic Toda lattice H_{D_4} in (2.2):

$$H_1 = H_{D_4}.$$

3.3 D_N

We start with two double impurity introduced to A_{2N-4} placed farthest away from each other. See Fig. 12 for illustration. The folding is performed in the according steps:

1. Set $\mathbf{q}_{2N-n+1} = -\mathbf{q}_n$, $\mathbf{p}_{2N-n+1} = -\mathbf{p}_{2N-n+1}$, $n = 1, \dots, N$. This gives $H_1 = H_{2N-1}$.
2. Change of canonical variables on the boundary of half-unit cell:

$$e^{\mathbf{q}_1} \rightarrow \frac{\sinh \mathbf{q}_1}{\cosh \frac{\mathbf{p}_1}{2}}, \quad e^{\mathbf{p}_1} \rightarrow \frac{\cosh \frac{\mathbf{p}_1 - 2\mathbf{q}_1}{2}}{\cosh \frac{\mathbf{p}_1 + 2\mathbf{q}_1}{2}}, \quad e^{\mathbf{q}_N} \rightarrow \frac{\cosh \frac{\mathbf{p}_N}{2}}{\sinh \mathbf{q}_N}, \quad e^{\mathbf{p}_N} \rightarrow \frac{\cosh \frac{\mathbf{p}_N + 2\mathbf{q}_N}{2}}{\cosh \frac{\mathbf{p}_N - 2\mathbf{q}_N}{2}}.$$

3. Modify the square loop as in (3.13).
4. The double impurity dimer now consists two identical copy of half unit cell, with one rotated by 180 degree.

The bipartite dimer diagram for D_N model in Fig. 13 based on the folding from the double impurity square dimer Fig. 12. All the 1-loops can be build by square loops and straight horizontal lines.

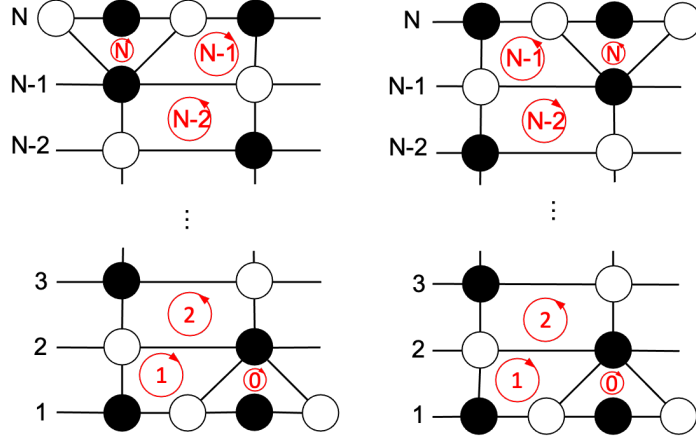


Figure 13. The dimer graph for D_N theory, even N on the left and odd N on the right, with the fundamental square loops labeled.

The square loops obeys the commutation relation

$$\begin{aligned} \{S_n, S_{n+1}\} &= (-1)^n S_n S_{n+1}, \quad n = 0, \dots, N-1 \\ \{S_n, e^{P_n}\} &= S_n e^{P_n}, \quad \{e^{P_{n+1}}, S_n\} = e^{P_{n+1}} S_n, \quad n = 1, \dots, N-1. \end{aligned} \quad (3.16)$$

The first Hamiltonian is the given by the sum over all 1-loops plus the two terms coming from connecting the two patchings:

$$\begin{aligned} H_1 &= \sum_{n=1}^N 2 \cosh p_n + \sum_{n=1}^{N-1} S_n (e^{-(-1)^n p_n} + e^{-(-1)^{n+1} p_{n+1}}) \\ &+ S_1 S_0 (e^{p_1} + e^{-p_2}) + S_{N-1} S_N (e^{-(-1)^{N-1} p_{N-1}} + e^{-(-1)^N p_N}) + e^{-2q_2} + e^{2q_{N-1}} \end{aligned} \quad (3.17)$$

We denote the square loops in terms of canonical coordinates to obey the Poisson commutation relation (3.16):

$$S_n = e^{q_n - q_{n+1}} e^{(-1)^n \frac{p_n - p_{n+1}}{2}}, \quad n = 1, \dots, N. \quad S_0 = e^{-2q_1}, \quad S_N = e^{2q_N}$$

We recover:

$$H_1|_{\text{dimer}} = H_{D_N}. \quad (3.18)$$

4 Lax formalism

4.1 Construct Lax matrix from dimer graph

A Kasteleyn matrix $K_{\mathbf{b}, \mathbf{w}}(X, Y)$ encodes the structure of a given dimer graph. The curve of the dimer graph is defined by

$$W(X, Y) = \det K_{\mathbf{b}, \mathbf{w}}(X, Y) = 0 \quad (4.1)$$

The curve, when properly weighted the dimer graph's edges with respect to the canonical coordinates, coincide with the spectral curve of the integrable system

$$\tilde{W}(X, Y) = \det(\mathbf{T}(X) - Y) = 0 \quad (4.2)$$

$\mathbf{T}(X)$ is the monodromy matrix of the relativistic integrable system in Sklyanin's Lax formalism [5].

The Kasteleyn matrix of $Y^{N,0}$ square dimer (Type A RTL) is a tri-diagonal $N \times N$ matrix.

$$K_{\mathbf{b}, \mathbf{w}, j} = \begin{cases} (h_i - \tilde{h}_i X), & j = i \in 2\mathbb{Z} + 1; \\ (h_i X^{-1} - \tilde{h}_i), & j = i \in 2\mathbb{Z}; \\ \tilde{v}_j Y^{-\delta_{j,1}}, & i = j - 1 \pmod{N}; \\ v_j Y^{\delta_{j,N}}, & i = j + 1, \pmod{N}; \\ 0, & \text{otherwise} \end{cases} \quad (4.3)$$

The 1-loops are constructed through the dimer edges

$$d_j = h_j \tilde{h}_j^{-1} = e^{p_j}, \quad c_j = h_j v_{j-1}^{-1} h_{j-1} \tilde{v}_j^{-1} = e^{\mathbf{q}_j - \mathbf{q}_{j+1}} e^{\frac{p_j + p_{j+1}}{2}} \quad (4.4)$$

The Lax matrix can be construct from the Kasteleyn of the dimer graph. We consider $N \times 1$ vector

$$\psi = \begin{pmatrix} \psi_1 \\ \vdots \\ \psi_N \end{pmatrix}, \quad K_{\mathbf{b}, \mathbf{w}} \psi = 0$$

Expanding the matrix equation gives N equations

$$\begin{aligned} (h_j - \tilde{h}_j X^{-1})\psi_j + v_{j-1}\psi_{j-1} + \tilde{v}_{j+1}\psi_{j+1} &= 0, \quad j \in 2\mathbb{Z} + 1; \\ (h_j X - \tilde{h}_j)\psi_j + v_{j-1}\psi_{j-1} + \tilde{v}_{j+1}\psi_{j+1} &= 0, \quad j \in 2\mathbb{Z}. \end{aligned} \quad (4.5)$$

with periodicity $\psi_{j+N} = Y\psi_j$. By shifting

$$\psi_j \rightarrow \begin{cases} \sqrt{X}\psi_j, & j \in 2\mathbb{Z} + 1 \\ \frac{1}{\sqrt{X}}\psi_j, & n \in 2\mathbb{Z}. \end{cases}$$

We obtain N equations

$$(X - h_j^{-1}\tilde{h}_j)\psi_j + \sqrt{X}h_j^{-1}(v_{j-1}\psi_{j-1} + \tilde{v}_{j+1}\psi_{j+1}) = 0. \quad (4.6)$$

Define

$$\Xi_j = \begin{pmatrix} \psi_j \\ \psi_{j-1} \end{pmatrix}. \quad (4.7)$$

The N equations (4.6) can be organized into N 2×2 matrix equations

$$\sqrt{X}h_j^{-1}\tilde{v}_{j+1}\Xi_{j+1} = \begin{pmatrix} X - h_j^{-1}\tilde{h}_j & -\sqrt{X}h_j^{-1}v_{j-1} \\ \sqrt{X}h_j^{-1}\tilde{v}_{j+1} & 0 \end{pmatrix} \Xi_j = \sqrt{X}h_j^{-1}L_j(X)\Xi_j. \quad (4.8)$$

By assigning the edges with canonical coordinate, we obtain

$$L_j(X) = \begin{pmatrix} 2 \sinh \frac{x-P_j}{2} & -e^{-q_j} \\ e^{q_j} & 0 \end{pmatrix} \quad (4.9)$$

The monodromy matrix is defined by

$$\mathbf{T}(X) = L_N(X) \cdots L_1(X), \quad \mathbf{T}(X)\Xi_1(X) = Y\Xi_1(X). \quad (4.10)$$

4.2 Reconstructing monodromy matrix from double impurity dimer

We consider the double impurity dimer 12. Notice that most of the part of the type D dimer is the same as the type A square dimer. The only difference comes from the double impurity introduced. See Fig. 14 for illustration. The sub-matrix of the full Kasteleyn matrix associated to a double impurity is

	3	2	1	0	0'	1'	2'	3'
2	s_{23}	$h_2X^{-1} - \tilde{h}_2$	s_{21}	s_{20}	0	0	0	0
1	0	s_{12}	h_1	$-s_{10}X$	0	0	0	0
0	0	0	$-s_{01}$	h_0	$\frac{s_{00'}Y}{X}$	$s_{01'}Y$	0	0
0'	0	0	$\frac{s_{0'1}}{Y}$	$\frac{s_{0'0}X}{Y}$	$-h_{0'}$	$s_{0'1'}$	0	0
1'	0	0	0	0	$\frac{s_{1'0'}}{X}$	$-h_{1'}$	$s_{1'2'}$	0
2'	0	0	0	0	$s_{2'0'}$	$s_{2'1'}$	$h_{2'} - \tilde{h}_{2'}X$	$s_{2'3'}$

Note that Y here labels the edge crosses HALF unit cell instead of the full unit cell. We would expect the spectral curve obtained from the Kasteleyn matrix as a function in Y^2 .

Consider the eigenvector $\psi = (\psi_N, \dots, \psi_0, \psi_{0'}, \dots, \psi_{N'})$ of the Kasteleyn matrix.

$$s_{23}\psi_3 + \left(\frac{h_2}{X} - \tilde{h}_2\right)\psi_2 + s_{21}\psi_1 + s_{20}\psi_0 = 0 \quad (4.11a)$$

$$s_{12}\psi_2 + h_1\psi_1 - s_{10}X\psi_0 = 0 \quad (4.11b)$$

$$-s_{01}\psi_1 + h_0\psi_0 + \frac{s_{00'}Y}{X}\psi_{0'} + s_{01'}Y\psi_{1'} = 0 \quad (4.11c)$$

$$\frac{s_{0'1}}{Y}\psi_1 + \frac{s_{0'0}X}{Y}\psi_0 - h_{0'}\psi_{0'} + s_{0'1'}\psi_{1'} = 0 \quad (4.11d)$$

$$\frac{s_{1'0'}}{X}\psi_{0'} - h_{1'}\psi_{1'} + s_{1'2'}\psi_{2'} = 0 \quad (4.11e)$$

$$s_{2'0'}\psi_{0'} + s_{2'1'}\psi_{1'} + \left(h_{2'} - \tilde{h}_{2'}X\right)\psi_{2'} + s_{2'3'}\psi_{3'} = 0 \quad (4.11f)$$

Taking third and fourth equations and we obtain:

$$(s_{01'}s_{0'1} + s_{0'1'}s_{01})\psi_1 + (s_{0'1'}h_0 + s_{0'0}s_{01'}X)\psi_0 + \left(-s_{01'}h_{0'} + \frac{s_{00'}s_{0'1'}}{X}\right)Y\psi_{0'} = 0 \quad (4.12a)$$

$$(s_{0'0}s_{01}X + s_{0'1}h_0)\frac{1}{Y}\psi_0 + \left(-s_{01}h_{0'} + \frac{s_{00'}s_{0'1}}{X}\right)\psi_{0'} + (s_{0'1}s_{01'} + s_{01}s_{0'1'})\psi_{1'} = 0 \quad (4.12b)$$

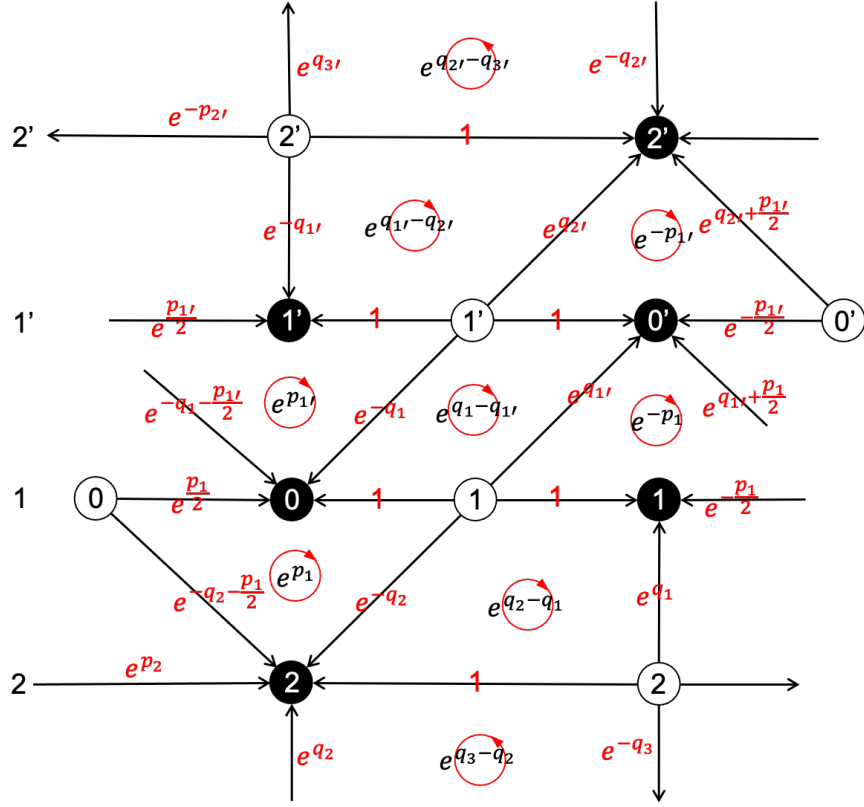


Figure 14. Assignment of the edges a weight associated to canonical coordinates which gives the correct loop contribution. Note that there exists more than one way to assign the edges. Different assignments are related by gauge transformation.

We will assign the edges according to Fig. 14.

We combine the matrices that transfers through the boundary by

$$\begin{aligned}
(1 - e^{-2q_1}) \frac{Y}{X} (X - 1)^2 \begin{pmatrix} \psi_2 \\ \tilde{\psi}_1 = \psi_1 + \frac{s_{20}}{s_{21}} \psi_0 \end{pmatrix} &= \begin{pmatrix} TL & TRs_{21} \\ BLs_{21} & BRs_{21}^2 \end{pmatrix} \begin{pmatrix} \psi_{1'} + \frac{s_{2'0'}}{s_{2'1'}} \psi_{0'} \\ \psi_{2'} \end{pmatrix} \\
&= (1 - e^{-2q_1}) \tilde{K}_1 \begin{pmatrix} \tilde{\psi}_{1'} = \psi_{1'} + \frac{s_{2'0'}}{s_{2'1'}} \psi_{0'} \\ \psi_{2'} \end{pmatrix}
\end{aligned} \tag{4.13}$$

The edges are assigned by canonical coordinates as in Fig. 14. We obtain:

$$TL = -(1 - e^{-2q_1}) \left[X + \frac{1}{X} - e^{-2q_1} (e^{p_1} - 2 + e^{-p_1}) - e^{p_1} - e^{-p_1} \right]$$

$$TR = -(1 - e^{-2q_1}) \left[(e^{-p_1} + 1)(1 - e^{-2q_1})X - (e^{p_1} + 1)(1 - e^{-2q_1}) \right]$$

$$BL = (1 - e^{-2q_1}) \left[(e^{-p_1} + 1)(1 - e^{-2q_1}) \frac{1}{X} - (e^{p_1} + 1)(1 - e^{-2q_1}) \right]$$

$$BR = (1 - e^{-2q_1}) \left[e^{-2q_1} \left(X + \frac{1}{X} \right) + (1 - e^{-2q_1})(e^{-p_1} + e^{p_1}) - 2 \right]$$

See Appendix. C for computational detail. We further take canonical coordinate transformation (3.12) and modifies $s_{21} = s_{2'1'}$ according to (3.13), which yields

$$\tilde{K}_1 = \begin{pmatrix} X + \frac{1}{X} - 2 \cosh 2q_1 & 2 \cosh \frac{p_1 - 2q_1}{2} X - 2 \cosh \frac{p_1 + 2q_1}{2} \\ -\frac{2}{X} \cosh \frac{p_1 - 2q_1}{2} + 2 \cosh \frac{p_1 + 2q_1}{2} & -X - \frac{1}{X} + 2 \cosh p_1 \end{pmatrix}. \quad (4.14)$$

Similarly for the other end of the half unit cell:

$$\tilde{K}_N = \begin{pmatrix} X + \frac{1}{X} - 2 \cosh 2q_N & 2 \cosh \frac{p_1 - 2q_N}{2} X - 2 \cosh \frac{p_N + 2q_N}{2} \\ -\frac{2}{X} \cosh \frac{p_N - 2q_N}{2} + 2 \cosh \frac{p_N + 2q_N}{2} & -X - \frac{1}{X} + 2 \cosh p_N \end{pmatrix}. \quad (4.15)$$

The monodromy matrix is defined by ordered product of the reflection matrices and Lax operators. By proper gauge transformation, we obtain

$$\mathbf{T}(X) = K_+(X) \tilde{L}_2(X) \cdots \tilde{L}_{N-1}(X) K_-(X) L_{N-1}(X) \cdots L_2(X) \quad (4.16)$$

where the Lax matrices and reflection matrices are given by

$$L_j(X) = \begin{pmatrix} 2 \sinh \frac{x-p_j}{2} & -e^{-p_j} \\ e^{p_j} & 0 \end{pmatrix}, \quad \tilde{L}_j(X) = \begin{pmatrix} 0 & e^{-q_j} \\ e^{q_j} & 2 \sinh \frac{x+p_j}{2} \end{pmatrix} \quad (4.17a)$$

$$K_+(X) = \begin{pmatrix} 2\sqrt{X} \cosh \frac{p_1 - 2q_1}{2} - \frac{2}{\sqrt{X}} \cosh \frac{p_1 + 2q_1}{2} & X + \frac{1}{X} - 2 \cosh 2q_1 \\ -X - \frac{1}{X} + 2 \cosh p_1 & 2\sqrt{X} \cosh \frac{p_1 + 2q_1}{2} - \frac{2}{\sqrt{X}} \cosh \frac{p_1 - 2q_1}{2} \end{pmatrix} \quad (4.17b)$$

$$K_-(X) = \begin{pmatrix} 2\sqrt{X} \cosh \frac{p_N + 2q_N}{2} - \frac{2}{\sqrt{X}} \cosh \frac{p_N - 2q_N}{2} & -X - \frac{1}{X} + 2 \cosh p_N \\ X + \frac{1}{X} - 2 \cosh 2q_N & 2\sqrt{X} \cosh \frac{p_1 - 2q_N}{2} - \frac{2}{\sqrt{X}} \cosh \frac{p_N + 2q_N}{2} \end{pmatrix} \quad (4.17c)$$

satisfying the eigen equation

$$\mathbf{T}(X) \begin{pmatrix} \psi_2 \\ \tilde{\psi}_1 \end{pmatrix} = Y^2 \left(X - \frac{1}{X} \right)^2 \begin{pmatrix} \psi_2 \\ \tilde{\psi}_1 \end{pmatrix} \quad (4.18)$$

The two components of the vector satisfies the spectral equation

$$\begin{aligned} Y^2(X - X^{-1})^2 \left[Y^2(X - X^{-1})^2 - \text{Tr} \mathbf{T}(X) + \frac{(X - X^{-1})^2}{Y^2} \right] \psi_2 &= 0 \\ Y^2(X - X^{-1})^2 \left[Y^2(X - X^{-1})^2 - \text{Tr} \mathbf{T}(X) + \frac{(X - X^{-1})^2}{Y^2} \right] \tilde{\psi}_1 &= 0 \end{aligned} \quad (4.19)$$

Recall that Y labels the crossing of half unit cell. Rescaling $Y^2 \rightarrow Y$ we recover the spectral curve in (2.24). In particular, we recover all the conserving Hamiltonian as the transfer matrix (trace of monodromy matrix) (2.17) is the generating function of all conserving Hamiltonians.

5 Summery and future directions

We construct dimer graph for the type D relativistic Toda lattice by introducing double impurity to the type A square dimer. A folding from type A with impurity to type D dimer is performed based on the identification of the faces and vertexes in the dimer unit cell, followed by a change of variable eq. (3.12) on the canonical variable across the impurity insertion square and modification of certain square loops by an overall factor (3.13). The first Hamiltonian of the double impurity dimer indeed reproduces the \hat{D}_N RTL.

Furthermore, we construct the Lax matrix and reflection matrix from the Kasteleyn matrix of the new dimer graph through the latter's Baker-Akhiezer function. Managing the Baker-Akhiezer function coefficient associated to the double impurity with proper assignment of the canonical coordinates on the edges on the dimer graph allows us to reconstruct both reflection matrices on the boundaries.

Let us end this note with some potential future direction:

- We are interested in the quantum type D RTL. Recent studies shows that Bethe/Gauge correspondence provides excellent tool particularly in solving the wavefunction of the quantum integrable system. It has been studied for various non-relativistic integrable systems [27–35]. It is known that the Nekrasov-Shatashvili free energy, which works excellently for 4D, is not enough to establish 5D Bethe/Gauge correspondence. The correct quantization requires including a tower of non-perturbative effects [36–38]. This can be done by introducing Wilson-loop/quantum mirror map by topological string [36, 39]. The off-shell quantization has been done for type A RTL in [9].
- Find potential dimer graph for type B, C and E RTL. We expect it can be done through proper introduction of impurity in the embedded type A dimer graph followed by folding.
- A Poisson graph (a quiver graph) can be constructed based on the blowup of the Lie algebra Dynkin diagram, studying the quiver gives the spectral property of the RTL [40]. In principle the dimer graph associated to the same RTL should be the dual graph of the Poisson graph. The relation is straight forward in the case of type A. The situation is more obscured for type BCDE as the dual of the quiver graph from Dynkin diagram are often not planar. It is an interesting topic to explore the potential relation between the dimer we constructed for type D with the Poisson graph.
- In this note we introduct double impurity placed furthest away based on the toric diagram shared by $A_{2N-1}/8F$ and D_N . As mentioned that this is not the only way one can modify the dimer graph to construct different but potentially dual integrable systems. Similar observation is found in [9].

A Lax formalism

Let briefly illustrate how type A periodic relativistic Toda lattice is associated to the $Y^{N,0}$ square dimer. We will also demonstrate how the $N \times N$ Lax matrix can be obtained from the dimer Kasteleyn matrix.

We choose the reference perfect matching on the $Y^{N,0}$ square dimer in Fig. 3 to be horizontal edges having white node on the left and black node on the right. There are $2N$ 1-loops $c_n, d_n, n = 1, \dots, N$ satisfying the commutation relation based on their shared edges:

$$\{c_n, d_n\} = c_n d_n, \quad \{d_{n+1}, c_n\} = c_n d_{n+1}, \quad \{c_n, c_{n+1}\} = -c_n c_{n+1}. \quad (\text{A.1})$$

with the periodicity $c_{N+1} = c_1, d_{N+1} = d_1$. See Fig. 15 for illustration.

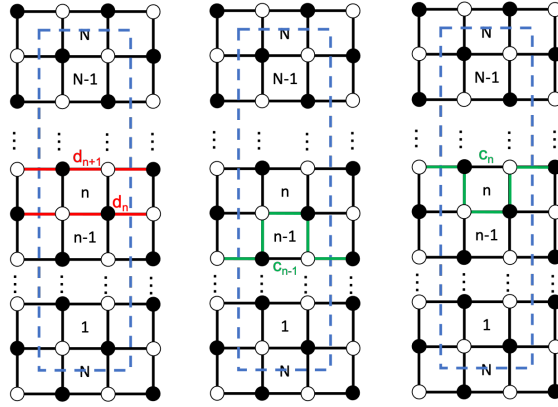


Figure 15. The brane tiling for $Y^{N,0}$ dimer model with N even. A unit cell is encircled by the dashed blue line. This dimer is associated to the \hat{A}_{N-1} relativistic Toda lattice.

The 1-loops can be written in terms of the canonical coordinates by

$$d_n = e^{\mathbf{p}n}, \quad c_n = e^{\mathbf{q}n - \mathbf{q}_{n+1}} e^{\frac{\mathbf{p}n + \mathbf{p}_{n+1}}{2}}, \quad n = 1, \dots, N. \quad (\text{A.2})$$

The canonical coordinates obeys the periodicity $\mathbf{q}_{N+1} = \mathbf{q}_1, \mathbf{p}_{N+1} = \mathbf{p}_1$. The first Hamiltonian of the $Y^{N,0}$ dimer graph recovers the \hat{A}_{N-1} RTL Hamiltonian

$$H_1|_{Y^{N,0}} = \sum_{n=1}^N c_n + d_n = \sum_{n=1}^N e^{\mathbf{p}n} + g^2 e^{\mathbf{q}n - \mathbf{q}_{n+1}} e^{\frac{\mathbf{p}n + \mathbf{p}_{n+1}}{2}} = \mathbf{H}_{\hat{A}_{N-1}} \quad (\text{A.3})$$

A.1 $N \times N$ Lax matrix

There are two ways to construct the Lax matrix of the integrable system from the dimer graph. The first one is by studying the equation of motion of the 1-loops, the second through Kasteleyn matrix of the dimer.

Equation of Motion: The equations of motion of the coordinates $\{c_n, d_n\}$ given by the Haamiltonian (A.3) have the following form

$$\begin{aligned}\dot{c}_n &= \{c_n, H_1\} = c_n(d_n - d_{n+1} + c_{n-1} - c_{n+1}), \\ \dot{d}_n &= \{d_n, H_1\} = d_n(c_{n-1} - c_n).\end{aligned}\tag{A.4}$$

and can be write as compatibility condition for the two linear problems [3, 18]

$$\begin{aligned}(X - d_j)\phi_j + \sqrt{X}(f_j\phi_{j+1} + f_{j-1}\phi_{j-1}) &= 0 \\ \dot{\phi}_j &= -\frac{1}{2}(c_j - c_{j-1} + X)\phi_j - \frac{\sqrt{X}}{2}(f_j\phi_{j+1} - f_{j-1}\phi_{j-1})\end{aligned}\tag{A.5}$$

It can be cast into matrix form

$$L\phi = 0, \quad \dot{\phi} = -M\phi\tag{A.6}$$

The Hamiltonian system obeys a "weak" Lax triad

$$\frac{d}{dt}L = [L, M] + CL\tag{A.7}$$

with the matrices

$$L_{ij} = (X - d_i)\delta_{i,j} + \sqrt{X}f_i\delta_{i+1,j} + \sqrt{X}f_{i-1}\delta_{i-1,j}\tag{A.8a}$$

$$M_{ij} = \frac{1}{2} \left[(c_i - c_{i-1} + X)\delta_{i,j} + \sqrt{X}f_i\delta_{i+1,j} - \sqrt{X}f_{i-1}\delta_{i-1,j} \right]\tag{A.8b}$$

$$C_{ij} = (c_i - c_{i-1})\delta_{i,j}\tag{A.8c}$$

with $f_i^2 = c_i$. The matrix C is diagonal and traceless. This leads to

$$\text{Tr}L^{-1}\frac{dL}{dt} = \text{Tr}L^{-1}([L, M] + CL) = \text{Tr}C = 0.\tag{A.9}$$

By using Abel identity

$$\frac{d}{dt} \log \det L = \text{Tr}L^{-1}\frac{dL}{dt} = 0$$

one concludes $\det L(X, Y)$ is the generating function of the integral of motion of RTL.

Kasteleyn matrix: The Kasteleyn matrix of square dimer in Fig.15 is

$$K_{\mathbf{b}_n, \mathbf{w}_m} = \begin{cases} (h_n - \tilde{h}_n X^{-1}), & n = m \in 2\mathbb{Z} + 1; \\ (h_n X - \tilde{h}_n), & n = m \in 2\mathbb{Z}; \\ \tilde{v}_m Y^{\delta_{m,1}}, & n = m - 1 \pmod{N}; \\ v_m Y^{-\delta_{m,N}}, & n = m + 1, \pmod{N}; \\ 0, & \text{otherwise} \end{cases}\tag{A.10}$$

The 1-loops are constructed through the dimer edges

$$d_n = h_n^{-1} \tilde{h}_n = e^{\mathfrak{p}_n}, \quad c_n = h_n^{-1} v_{n-1} h_{n-1}^{-1} \tilde{v}_n = e^{\mathfrak{q}_n - \mathfrak{q}_{n+1}} e^{\frac{\mathfrak{p}_n + \mathfrak{p}_{n+1}}{2}}. \quad (\text{A.11})$$

We consider $N \times 1$ vector

$$\boldsymbol{\psi} = \begin{pmatrix} \psi_1 \\ \psi_2 \\ \vdots \\ \psi_N \end{pmatrix}, \quad K_{\mathbf{b}, \mathbf{w}} \boldsymbol{\psi} = 0$$

Expanding the matrix equation gives N equations

$$\begin{aligned} (h_n - \tilde{h}_n X^{-1}) \psi_n + v_{n-1} \psi_{n-1} + \tilde{v}_{n+1} \psi_{n+1} &= 0, \quad n \in 2\mathbb{Z} + 1; \\ (h_n X - \tilde{h}_n) \psi_n + v_{n-1} \psi_{n-1} + \tilde{v}_{n+1} \psi_{n+1} &= 0, \quad n \in 2\mathbb{Z}. \end{aligned} \quad (\text{A.12})$$

with periodicity $\psi_{n+N} = y \psi_n$. By shifting

$$\psi_n \rightarrow \begin{cases} \sqrt{X} \psi_n, & n \in 2\mathbb{Z} + 1 \\ \frac{1}{\sqrt{X}} \psi_n, & n \in 2\mathbb{Z}. \end{cases}$$

We obtain N equations

$$(X - h_n^{-1} \tilde{h}_n) \psi_n + \sqrt{X} h_n^{-1} (v_{n-1} \psi_{n-1} + \tilde{v}_{n+1} \psi_{n+1}) = 0 \quad (\text{A.13})$$

which can be organized into a matrix equation

$$\tilde{L} \boldsymbol{\psi} = 0, \quad \tilde{L}_{nm} = (X - h_n^{-1} \tilde{h}_n) \delta_{n,m} + \sqrt{X} h_n^{-1} (v_{n-1} \delta_{n-1,m} + \tilde{v}_{n+1} \delta_{n+1,m}) \quad (\text{A.14})$$

We further conjugate diagonal matrix $A = \text{diag}(a_1, \dots, a_N)$ with

$$\frac{a_n}{a_{n-1}} = \sqrt{\frac{\tilde{v}_n h_n}{v_{n-1} h_{n-1}}}$$

to obtain

$$L_{nm} = (A \tilde{L} A^{-1})_{nm} = (X - d_n) \delta_{nm} + \sqrt{X} (f_n \delta_{n-1,m} + f_{n+1} \delta_{n+1,m}) \quad (\text{A.15})$$

with $f_n^2 = c_n$.

A.2 2×2 Lax matrix

The 2×2 Lax formalism proposed by Sklyanin is equivalent to the $N \times N$ Lax matrix. Define 2×1 vector

$$\Xi_n = \begin{pmatrix} \psi_n \\ \psi_{n-1} \end{pmatrix} \quad (\text{A.16})$$

The N equations (4.6) can be organized into N 2×2 matrix equation

$$\sqrt{X} h_n^{-1} \tilde{v}_{n+1} \Xi_{n+1} = \begin{pmatrix} X - h_n^{-1} \tilde{h}_n & -\sqrt{X} h_n^{-1} v_{n-1} \\ \sqrt{X} h_n^{-1} \tilde{v}_{n+1} & 0 \end{pmatrix} \Xi_n = \sqrt{X} h_n^{-1} L_n(X) \Xi_n \quad (\text{A.17})$$

The monodromy matrix is defined by

$$\mathbf{T}(X) = L_N(x) \cdots L_1(X). \quad (\text{A.18})$$

B Canonical change of variables

Let us check the change of variables in (3.12) is canonical by direct computation:

$$\begin{aligned}
e^q e^p &= \{e^q, e^p\} \\
&\rightarrow \left\{ \frac{\cosh \frac{p}{2}}{\sinh q}, \frac{\cosh \frac{p-2q}{2}}{\cosh \frac{p+2q}{2}} \right\} \\
&= \frac{\partial \cosh \frac{p}{2}}{\partial q \sinh q} \frac{\partial \cosh \frac{p-2q}{2}}{\partial p \cosh \frac{p+2q}{2}} - \frac{\partial \cosh \frac{p-2q}{2}}{\partial q \cosh \frac{p+2q}{2}} \frac{\partial \cosh \frac{p}{2}}{\partial p \sinh q} \\
&= -\frac{\cosh \frac{p}{2} \cosh q}{\sinh^2 q} \frac{1}{2} \frac{\sinh \frac{p-2q}{2} \cosh \frac{p+2q}{2} - \cosh \frac{p-2q}{2} \sinh \frac{p+2q}{2}}{\cosh^2 \frac{p+2q}{2}} \\
&\quad + \frac{\sinh \frac{p-2q}{2} \cosh \frac{p+2q}{2} + \cosh \frac{p-2q}{2} \sinh \frac{p+2q}{2}}{\cosh^2 \frac{p+2q}{2}} \frac{1}{2} \frac{\sinh \frac{p}{2}}{\sinh q} \\
&= \frac{1}{2} \frac{\sinh p \sinh \frac{p}{2} \sinh q + \cosh \frac{p}{2} \cosh q \sinh 2q}{\sinh^2 q \cosh^2 \frac{p+2q}{2}} \\
&= \frac{\cosh \frac{p}{2} \sinh^2 \frac{p}{2} + \cosh \frac{p}{2} \cosh^2 q}{\sinh q \cosh^2 \frac{p+2q}{2}} \\
&= \frac{\cosh \frac{p}{2} \cosh \frac{p-2q}{2}}{\sinh q \cosh \frac{p+2q}{2}}
\end{aligned} \tag{B.1}$$

C Detail computation in section 4.2

The six components of the Kasteleyn matrix Baker-Akzeihier function (4.11) across the double impurity insertion can be organized into six matrix equations

$$s_{23} \begin{pmatrix} \psi_3 \\ \psi_2 \end{pmatrix} = \begin{pmatrix} \tilde{h}_2 - \frac{h_2}{X} & -s_{21} \\ s_{23} & 0 \end{pmatrix} \begin{pmatrix} \psi_2 \\ \psi_1 + \frac{s_{20}}{s_{21}} \psi_0 \end{pmatrix} \tag{C.1a}$$

$$s_{12} \begin{pmatrix} \psi_2 \\ \psi_1 + \frac{s_{20}}{s_{21}} \psi_0 \end{pmatrix} = \begin{pmatrix} -h_1 & s_{10} X \\ s_{12} & s_{12} \frac{s_{20}}{s_{21}} \end{pmatrix} \begin{pmatrix} \psi_1 \\ \psi_0 \end{pmatrix} \tag{C.1b}$$

$$(-s_{0'1'} s_{01} - s_{01'} s_{0'1}) \begin{pmatrix} \psi_1 \\ \psi_0 \end{pmatrix} = \begin{pmatrix} s_{0'1'} h_0 + s_{0'0} s_{01'} X & h_{0'} s_{01'} + \frac{s_{00'} s_{0'1'}}{X} \\ -s_{0'1'} s_{01} - s_{01'} s_{0'1} & 0 \end{pmatrix} \begin{pmatrix} \psi_0 \\ Y \psi_{0'} \end{pmatrix} \tag{C.1c}$$

$$\frac{1}{Y} (s_{01} s_{0'0} X + h_0 s_{0'1}) \begin{pmatrix} \psi_0 \\ Y \psi_{0'} \end{pmatrix} = \begin{pmatrix} h_{0'} s_{01} - \frac{s_{00'} s_{0'1}}{X} & -s_{01} s_{0'1'} - s_{0'1} s_{01'} \\ s_{01} s_{0'0} X + h_0 s_{0'1} & 0 \end{pmatrix} \begin{pmatrix} \psi_{0'} \\ \psi_{1'} \end{pmatrix} \tag{C.1d}$$

$$(s_{2'0'} h_{1'} X - s_{1'0'} s_{2'1'}) \begin{pmatrix} \psi_{0'} \\ \psi_{1'} \end{pmatrix} = X s_{2'1'} \begin{pmatrix} -h_{1'} & s_{1'2'} \\ -\frac{s_{1'0'}}{X} & -s_{1'2'} \frac{s_{2'0'}}{s_{2'1'}} \end{pmatrix} \begin{pmatrix} \psi_{1'} + \frac{s_{2'0'}}{s_{2'1'}} \psi_{0'} \\ \psi_{2'} \end{pmatrix} \tag{C.1e}$$

$$s_{2'1'} \begin{pmatrix} \psi_{1'} + \frac{s_{2'0'}}{s_{2'1'}} \psi_{0'} \\ \psi_{2'} \end{pmatrix} = \begin{pmatrix} \tilde{h}_{2'} X - h_{2'} & -s_{2'3'} \\ s_{2'1'} & 0 \end{pmatrix} \begin{pmatrix} \psi_{2'} \\ \psi_{3'} \end{pmatrix} \tag{C.1f}$$

We will combine the matrices in the second to fifth line

$$\begin{aligned}
& \begin{pmatrix} -h_1 & s_{10}X \\ s_{12} & s_{12}\frac{s_{20}}{s_{21}} \end{pmatrix} \begin{pmatrix} s_{0'1}h_0 + s_{0'0}s_{01}X & h_{0'}s_{01'} + \frac{s_{00'}s_{0'1'}}{X} \\ -s_{0'1'}s_{01} - s_{01'}s_{0'1} & 0 \end{pmatrix} \\
& \times \begin{pmatrix} h_{0'}s_{01} - \frac{s_{00'}s_{0'1}}{X} & -s_{01}s_{0'1'} - s_{0'1}s_{01'} \\ s_{01}s_{0'0}X + h_0s_{0'1} & 0 \end{pmatrix} \begin{pmatrix} -h_{1'} & s_{1'2'} \\ -\frac{s_{1'0'}}{X} & -s_{1'2'}\frac{s_{2'0'}}{s_{2'1'}} \end{pmatrix} \\
& = \begin{pmatrix} 1 & 0 \\ 0 & s_{12} \end{pmatrix} \begin{pmatrix} -[s_{10}(s_{01}s_{0'1'} + s_{0'1}s_{01}) + h_1s_{0'0}s_{01'}]X - h_1h_0s_{0'1'} - h_1h_{0'}s_{01'} - \frac{h_1s_{00'}s_{0'1'}}{X} \\ s_{0'0}s_{01'}X + s_{0'1}h_0 - (s_{01}s_{0'1'} + s_{0'1}s_{01})\frac{s_{20}}{s_{21}} & h_{0'}s_{01'} + \frac{s_{00'}s_{0'1'}}{X} \end{pmatrix} \\
& \times \begin{pmatrix} -h_0h_1s_{01} + \frac{(s_{01}s_{0'1'} + s_{0'1}s_{01})s_{1'0'} + h_1's_{00'}s_{0'1}}{X} & [h_0s_{01} + (s_{01}s_{0'1'} + s_{0'1}s_{01})\frac{s_{20}}{s_{21}}] - \frac{s_{00'}s_{01'}}{X} \\ -h_{1'}s_{01}s_{0'0}X - h_{1'}h_0s_{0'1} & s_{01}s_{0'0}X + h_0s_{0'1} \end{pmatrix} \begin{pmatrix} 1 & 0 \\ 0 & s_{12} \end{pmatrix} \\
& = \begin{pmatrix} TL & TRs_{12} \\ BLs_{12} & BRs_{12}^2 \end{pmatrix}
\end{aligned} \tag{C.2}$$

The folding restricts:

$$h_0 = h_{0'}, \quad h_1 = h_{1'}, \quad s_{01} = s_{0'1'}, \quad s_{10} = s_{1'0'}, \quad s_{12} = s_{1'2'}, \quad s_{01'} = s_{0'1}, \quad s_{0'0} = s_{00'}.$$

$$\begin{aligned}
& \begin{pmatrix} 1 & 0 \\ 0 & s_{12} \end{pmatrix} \begin{pmatrix} [s_{10}(s_{01}s_{0'1'} - s_{0'1}s_{01}) - h_1s_{0'0}s_{01'}]X - h_1h_0s_{0'1'} - h_1h_{0'}s_{01'} - \frac{h_1s_{00'}s_{0'1'}}{X} \\ s_{0'0}s_{01'}X + s_{0'1}h_0 + (s_{01}s_{0'1'} - s_{0'1}s_{01})\frac{s_{20}}{s_{21}} & h_{0'}s_{01'} + \frac{s_{00'}s_{01}}{X} \end{pmatrix} \\
& \times \begin{pmatrix} -h_0h_1s_{01} + \frac{(s_{01}^2 - s_{0'1}s_{01'})s_{10} - h_1s_{00'}s_{0'1}}{X} & [h_0s_{01} + (s_{01}^2 - s_{0'1}s_{01'})\frac{s_{20}}{s_{21}}] - \frac{s_{00'}s_{01'}}{X} \\ h_1s_{01}s_{0'0}X + h_1h_0s_{0'1} & s_{01}s_{0'0}X + h_0s_{0'1} \end{pmatrix} \begin{pmatrix} 1 & 0 \\ 0 & s_{12} \end{pmatrix} \\
& = \begin{pmatrix} TL & TRs_{12} \\ BLs_{12} & BRs_{12}^2 \end{pmatrix}
\end{aligned} \tag{C.3}$$

$$\begin{aligned}
TL & = -(s_{01}^2 - s_{0'1}s_{01'})h_0h_1s_{01}s_{10} \left(X + \frac{1}{X} \right) \\
& \quad + (s_{10}s_{01}^2 - s_{10}s_{0'1}s_{0'1} - h_1s_{0'0}s_{01'})^2 + h_0^2h_1^2(s_{01}^2 - s_{0'1}s_{01'}) - h_1^2s_{01}^2s_{00'}s_{0'0} \\
& = (s_{01}^2 - s_{0'1}^2) \left[-s_{01}s_{10}h_0h_1 \left(X + \frac{1}{X} \right) + s_{10}^2(s_{01}^2 - s_{0'1}^2) - 2s_{0'0}s_{01'}h_1s_{10} + h_0^2h_1^2 - h_1^2s_{00'}^2 \right]
\end{aligned} \tag{C.4}$$

$$\begin{aligned}
TR &= \left[-(s_{10}s_{01}^2 - s_{10}s_{01'}s_{0'1} - h_1s_{0'0}s_{01'}) \left(h_0s_{01} + (s_{01}^2 - s_{01'}s_{0'1}) \frac{s_{20}}{s_{21}} \right) - h_1h_0s_{01'}s_{01}s_{0'0} \right] X \\
&\quad + [h_1h_0s_{01}s_{00'}s_{01'} - h_1h_0s_{00'}s_{01}s_{01'}] \frac{1}{X} \\
&\quad - (s_{10}(s_{01}^2 - s_{01'}s_{0'1}) - h_1s_{0'0}s_{01'})s_{00'}s_{01'} + h_1h_0s_{01} \left(h_0s_{01} + (s_{01}^2 - s_{01'}s_{0'1}) \frac{s_{20}}{s_{21}} \right) \\
&\quad - h_1h_0^2s_{01'}s_{0'1} - h_1s_{00'}s_{0'0}s_{01}^2 \\
&= (s_{01}^2 - s_{0'1}^2) \left[-\frac{s_{10}s_{20}}{s_{21}}(s_{01}^2 - s_{0'1}^2) - h_0s_{01}s_{10} + h_1s_{0'0}s_{01'} \frac{s_{20}}{s_{21}} \right] X \\
&\quad + (s_{01}^2 - s_{0'1}^2) \left[h_1h_0^2 - h_1s_{00'}s_{0'0} - s_{10}s_{00'}s_{01'} + h_1h_0s_{01} \frac{s_{20}}{s_{21}} \right]
\end{aligned} \tag{C.5}$$

$$\begin{aligned}
BL &= [-h_1h_0s_{01}s_{0'0}s_{01'} + h_1h_0s_{0'1}s_{0'0}s_{01}]X \\
&\quad + \left[(s_{10}(s_{01}^2 - s_{01'}s_{0'1}) - h_1s_{00'}s_{0'1}) \left(h_0s_{01} + (s_{01}^2 - s_{01'}s_{0'1}) \frac{s_{20}}{s_{21}} + h_1h_0s_{01'}s_{01}s_{0'0} \right) \right] \frac{1}{X} \\
&\quad + ((s_{01}^2 - s_{01'}s_{0'1})s_{10} - h_1s_{00'}s_{0'1})s_{0'0}s_{01'} - h_0h_1s_{01} \left(h_0s_{01} + (s_{01}^2 - s_{01'}s_{0'1}) \frac{s_{20}}{s_{21}} \right) \\
&\quad + h_1s_{01}^2s_{00'}s_{0'0} + h_0^2h_1s_{0'1}s_{01'} \\
&= (s_{01}^2 - s_{0'1}^2) \left[\frac{s_{10}s_{20}}{s_{21}}(s_{01}^2 - s_{0'1}^2) + h_0s_{01}s_{10} - h_1s_{00'}s_{0'1} \frac{s_{20}}{s_{21}} \right] \frac{1}{X} \\
&\quad + (s_{01}^2 - s_{0'1}^2) \left[-h_1h_0^2 + h_1s_{00'}s_{0'0} + s_{10}s_{00'}s_{01'} - h_1h_0s_{01} \frac{s_{20}}{s_{21}} \right]
\end{aligned} \tag{C.6}$$

$$\begin{aligned}
BR &= -s_{0'0}s_{01'}(s_{01}^2 - s_{01'}s_{0'1}) \frac{s_{20}}{s_{21}} \left(X + \frac{1}{X} \right) \\
&\quad - \left(h_0s_{01} + (s_{01}^2 - s_{01'}s_{0'1}) \frac{s_{20}}{s_{21}} \right)^2 - s_{0'0}s_{01'}s_{00'}s_{01'} + h_0^2s_{01'}s_{0'1} + s_{00'}s_{0'0}s_{01}^2 \\
&= (s_{01}^2 - s_{0'1}^2) \left[-s_{0'0}s_{01'} \frac{s_{20}}{s_{21}} \left(X + \frac{1}{X} \right) + (s_{01}^2 - s_{0'1}^2) \frac{s_{20}^2}{s_{21}^2} - 2h_0s_{01} \frac{s_{20}}{s_{21}} + s_{00'}s_{0'0} - h_0^2 \right]
\end{aligned}$$

We assign the edges on the double impurity according to Fig. 14. We obtain:

$$\begin{aligned}
TL &= -(1 - e^{-2q_1}) \left[X + \frac{1}{X} - e^{-2q_1}(e^{p_1} - 2 + e^{-p_1}) - e^{p_1} - e^{-p_1} \right] \\
TR &= -(1 - e^{-2q_1}) \left[(e^{-p_1} + 1)(1 - e^{-2q_1})X - (e^{p_1} + 1)(1 - e^{-2q_1}) \right] \\
BL &= (1 - e^{-2q_1}) \left[(e^{-p_1} + 1)(1 - e^{-2q_1}) \frac{1}{X} - (e^{p_1} + 1)(1 - e^{-2q_1}) \right] \\
BR &= (1 - e^{-2q_1}) \left[e^{-2q_1} \left(X + \frac{1}{X} \right) + (1 - e^{-2q_1})(e^{-p_1} + e^{p_1}) - 2 \right]
\end{aligned}$$

References

- [1] S. Ruijsenaars, “Relativistic toda systems,”
- [2] O. Ragnisco and M. Bruschi, “The periodic relativistic toda lattice: direct and inverse problem,” *Inverse Problems* **5** no. 3, (1989) 389.
- [3] M. Bruschi and O. Ragnisco, “Lax representation and complete integrability for the periodic relativistic toda lattice,” *Physics Letters A* **134** no. 6, (1989) 365–370.
- [4] E. K. Sklyanin, “Boundary conditions for integrable quantum systems,” *Journal of Physics A: Mathematical and General* **21** no. 10, (1988) 2375.
- [5] E. K. Sklyanin, “Separation of variables: new trends,” *Progress of Theoretical Physics Supplement* **118** (1995) 35–60.
- [6] A. B. Goncharov and R. Kenyon, “Dimers and cluster integrable systems,” *arXiv preprint arXiv:1107.5588* (2011) .
- [7] R. Eager, S. Franco, and K. Schaeffer, “Dimer Models and Integrable Systems,” *JHEP* **06** (2012) 106, [arXiv:1107.1244 \[hep-th\]](#).
- [8] A. Hanany and K. D. Kennaway, “Dimer models and toric diagrams,” [arXiv:hep-th/0503149](#).
- [9] N. Lee, “New dimer integrable systems and defects in five dimensional gauge theory,” [arXiv:2312.13133 \[hep-th\]](#).
- [10] A. Gorsky and A. Mironov, “Solutions to the reflection equation and integrable systems for N=2 SQCD with classical groups,” *Nucl. Phys. B* **550** (1999) 513–530, [arXiv:hep-th/9902030](#).
- [11] A. Gorsky, S. Gukov, and A. Mironov, “Multiscale N=2 SUSY field theories, integrable systems and their stringy / brane origin. 1.,” *Nucl. Phys. B* **517** (1998) 409–461, [arXiv:hep-th/9707120](#).
- [12] A. Gorsky and A. Mironov, “Integrable many body systems and gauge theories,” [arXiv:hep-th/0011197](#).
- [13] R. Donagi and E. Witten, “Supersymmetric Yang-Mills theory and integrable systems,” *Nucl. Phys. B* **460** (1996) 299–334, [arXiv:hep-th/9510101](#).
- [14] N. Nekrasov, “Five dimensional gauge theories and relativistic integrable systems,” *Nucl. Phys. B* **531** (1998) 323–344, [arXiv:hep-th/9609219](#).
- [15] H. Hayashi, S.-S. Kim, K. Lee, and F. Yagi, “Seiberg-Witten curves with $O7^\pm$ -planes,” [arXiv:2306.11631 \[hep-th\]](#).
- [16] O. I. Bogoyavlensky, “On perturbations of the periodic toda lattice,” *Communications in Mathematical Physics* **51** (1976) 201–209.
- [17] V. Kuznetsov and A. Tsyganov, “Infinite series of lie algebras and boundary conditions for integrable systems,” *Journal of Soviet Mathematics* **59** (1992) 1085–1092.
- [18] V. B. Kuznetsov and A. V. Tsyganov, “Separation of variables for the quantum relativistic Toda lattices,” [arXiv:hep-th/9402111](#).
- [19] N. Iorgov, V. Roubtsov, V. Shadura, and Y. Tykhyy, “Relativistic Toda chain with boundary interaction at root of unity,” [arXiv:nlin/0701040](#).

- [20] H. J. de Vega and A. Gonzalez-Ruiz, “Boundary K matrices for the XYZ, XXZ and XXX spin chains,” *J. Phys. A* **27** (1994) 6129–6138, [arXiv:hep-th/9306089](#).
- [21] E. J. Martinec and N. P. Warner, “Integrable systems and supersymmetric gauge theory,” *Nucl. Phys. B* **459** (1996) 97–112, [arXiv:hep-th/9509161](#).
- [22] R. Kenyon, “An introduction to the dimer model,” *arXiv preprint math/0310326* (2003) .
- [23] S. Franco, A. Hanany, K. D. Kennaway, D. Vegh, and B. Wecht, “Brane dimers and quiver gauge theories,” *JHEP* **01** (2006) 096, [arXiv:hep-th/0504110](#).
- [24] S. Benvenuti, A. Hanany, and P. Kazakopoulos, “The Toric phases of the $Y^{**p,q}$ quivers,” *JHEP* **07** (2005) 021, [arXiv:hep-th/0412279](#).
- [25] M.-x. Huang, Y. Sugimoto, and X. Wang, “Quantum periods and spectra in dimer models and Calabi-Yau geometries,” *JHEP* **09** (2020) 168, [arXiv:2006.13482](#) [[hep-th](#)].
- [26] D. Treumann, H. Williams, and E. Zaslow, “Kasteleyn operators from mirror symmetry,” *Selecta Mathematica* **25** (2019) 1–36.
- [27] N. Nekrasov, “BPS/CFT correspondence V: BPZ and KZ equations from qq -characters,” [arXiv:1711.11582](#) [[hep-th](#)].
- [28] S. Jeong, N. Lee, and N. Nekrasov, “Parallel surface defects, Hecke operators, and quantum Hitchin system,” [arXiv:2304.04656](#) [[hep-th](#)].
- [29] S. Jeong, N. Lee, and N. Nekrasov, “Intersecting defects in gauge theory, quantum spin chains, and Knizhnik-Zamolodchikov equations,” *JHEP* **10** (2021) 120, [arXiv:2103.17186](#) [[hep-th](#)].
- [30] H.-Y. Chen, T. Kimura, and N. Lee, “Quantum Elliptic Calogero-Moser Systems from Gauge Origami,” *JHEP* **02** (2020) 108, [arXiv:1908.04928](#) [[hep-th](#)].
- [31] H.-Y. Chen, T. Kimura, and N. Lee, “Quantum Integrable Systems from Supergroup Gauge Theories,” *JHEP* **09** (2020) 104, [arXiv:2003.13514](#) [[hep-th](#)].
- [32] N. Lee and N. Nekrasov, “Quantum spin systems and supersymmetric gauge theories. Part I,” *JHEP* **03** (2021) 093, [arXiv:2009.11199](#) [[hep-th](#)].
- [33] S. Jeong, “Splitting of surface defect partition functions and integrable systems,” *Nucl. Phys. B* **938** (2019) 775–806, [arXiv:1709.04926](#) [[hep-th](#)].
- [34] S. Jeong, N. Lee, and N. Nekrasov, “di-Langlands correspondence and extended observables,” [arXiv:2402.13888](#) [[hep-th](#)].
- [35] S. Jeong and N. Lee, “Bispectral duality and separation of variables from surface defect transition,” [arXiv:2402.13889](#) [[hep-th](#)].
- [36] A. Grassi, Y. Hatsuda, and M. Marino, “Topological Strings from Quantum Mechanics,” *Annales Henri Poincare* **17** no. 11, (2016) 3177–3235, [arXiv:1410.3382](#) [[hep-th](#)].
- [37] S. Franco, Y. Hatsuda, and M. Mariño, “Exact quantization conditions for cluster integrable systems,” *J. Stat. Mech.* **1606** no. 6, (2016) 063107, [arXiv:1512.03061](#) [[hep-th](#)].
- [38] Y. Hatsuda and M. Marino, “Exact quantization conditions for the relativistic Toda lattice,” *JHEP* **05** (2016) 133, [arXiv:1511.02860](#) [[hep-th](#)].
- [39] A. Grassi and M. Marino, “The complex side of the TS/ST correspondence,” *J. Phys. A* **52** no. 5, (2019) 055402, [arXiv:1708.08642](#) [[hep-th](#)].

- [40] O. Kruglinskaya and A. Marshakov, “On Lie Groups and Toda Lattices,” *J. Phys. A* **48** no. 12, (2015) 125201, [arXiv:1404.6507 \[hep-th\]](#).